THE INFLUENCE OF MAGNETIC FIELDS ON THE THERMAL CONDUCTIVITY OF NITROGEN AT LOW TEMPERATURES

An Abstract of a Thesis

Presented to

the Faculty of the Department of Chemical Engineering

University of Houston

In Partial Fulfillment

of the Requirements for the Degree

Master of Science in Chemical Engineering

---

by

Jehangir Erach Vevai

August, 1970

ACKNOWLEDGEMENTS

I wish to express my appreciation to the faculty of the Chemical Engineering Department and, particularly, to Dr. Wallace I. Honeywell for their guidance and encouragement. Also, I extend my thanks to my colleagues, Mr. Douglas G. Elliot and Mr. Louis E. Stein, for their many hours of assistance in the laboratory and to Messers Roy Priest and Lee Bennett for their advice and help in fabricating the experimental apparatus.

Finally, I wish to thank the National Science Foundation for financing the project.

THE INFLUENCE OF MAGNETIC FIELDS ON THE THERMAL CONDUCTIVITY OF NITROGEN AT LOW TEMPERATURES

An Abstract of a Thesis

Presented to

the Faculty of the Department of Chemical Engineering

University of Houston

In Partial Fulfillment

of the Requirements for the Degree

Master of Science in Chemical Engineering

---

by

Jehangir Erach Vevai

August, 1970

ABSTRACT

A concentric cylinder type of thermal conductivity apparatus with small "end effects" was designed, constructed and used to measure the effect of magnetic fields on the thermal conductivity of nitrogen gas at 78°K. A resolution of 10^{-5} in relative thermal conductivity was obtained. The axis of the cell was perpendicular to the field, H, produced by an electromagnet. Knudsen effects were found to be small enough at the operating pressures, p, --0.25 to 8.0 Torr.--so that the effect was a unique function of H/p. During the experiment, 90% of the saturation of the effect was attained. Extrapolation yielded a somewhat lower saturation value of the effect, and a considerably larger $(H/p)_{\frac{1}{2}}$ than those obtained at room temperature by other investigators. But, the ratio of the "experimental" collision integral to the one obtained by the elastic collision theory showed no significant differences.

A study was made to determine the effect of magnetic fields on the electrical resistance of various temperature sensors and lead materials. Significant effects were found for most of them, especially at low temperatures. The data were linearized and compared to determine the most suitable materials. Based on the data, procedures were devised to effectively eliminate the magnetoresistance effects on the temperature sensors and the leads.

TABLE OF CONTENTS

Chapter Page

Page

LIST OF TABLES

LIST OF FIGURES

Figure Page

CHAPTER I

INTRODUCTION

The collisional mechanics of dilute monatomic gases have been well understood for some time now, and the physical properties of such gases have been satisfactorily predicted by the theories available. This is not however the case for polyatomic gases.

The main hurdle is that polyatomic gases possess internal degrees of freedom and hence undergo elastic as well as inelastic collisions. An inelastic collision is one during which a transfer takes place between the translational energy and the internal energy of the colliding molecules; hence, translational energy is no longer conserved. The situation is further aggravated by the absence of a physical property that is significantly affected by the non-sphericity of the intermolecular interactions. It may be noted in this context that the thermal conductivity and viscosity is affected only in the second order by the non-sphericity[4].

Fortunately, however, due to the pioneering work of Senftleben[5-7] (1930), a new tool has been found. He discovered that when paramagnetic gases like oxygen and nitric oxide were subjected to a magnetic field, they showed a small reduction in their thermal conductivities and viscosities. Much later, in 1962, Beenakker, et.al.[4] showed that the

effect was not restricted to paramagnetic gases alone but was a general property of all polyatomic gases. The effect is now called the "Senftleben-Beenakker Effect." (Henceforth to be denoted by "S-B Effect.")

The S-B effect is always very small--of the order of a per cent at its largest--and hence difficult to measure. Nevertheless, it merits detailed experimental investigation because it depends entirely upon the internal structure of molecules and the non-central contributions towards the intermolecular interactions. Also, the effect is quite sensitive to inelastic collisions. Hence, S-B effect data provide us with a powerful method of checking various theories and models of dilute gas dynamics.

It may be mentioned in passing that the "Scott Effect" named after its discoverer, Scott[8] (1967), could be used to serve much the same purpose in the rarified gas regime. He showed that a heated metallic cylinder suspended in a rarified polyatomic gas experienced a torque if placed in a magnetic field.

A QUALITATIVE EXPLANATION OF THE SENFTLEBEN-BEENAKKER EFFECT.

In 1938, Gorter[9] suggested a simple mean free path interpretation which was expounded qualitatively by Zernike and van Lier[10] (1939). They pictured the rapidly rotating polyatomic molecules to be like discs with a magnetic moment, $\overline{\mu}$,

along the axis of rotation. The collisional cross section of such molecules would then be a function of the angle, α, between the velocity vector, $\overline{v}$, and the magnetic moment vector. In the zero field case, α was obviously constant between collisions. However, in the presence of a magnetic field, it was proposed that the magnetic moment vector would precess about the field vector, $\overline{H}$. This phenomenon is called Larmor precession. The result in this case is that α would vary periodically and so would the

Zero Field Finite Field

Figure 1. The Effect of a Magnetic Field on a Rotating Polyatomic Molecule

collision cross section. It was shown that even though the velocity vectors are randomly distributed with respect to the direction of the field, the net result is an effective increase in the overall collision cross section, causing a decrease in the mean free path, and hence a decrease in the transport coefficients, namely the thermal conductivity and the viscosity.

The Larmor precession frequency, ω_L, is proportional to the product of the field and the magnetic moment. Hence, as

the field becomes stronger, ω_L increases. When it becomes very large as compared to the collision frequency, τ^{-1}, i.e., when $\omega_L \tau >> 1$, the effect may be expected to reach a maximum steady value. Also, the larger the nonsphericity of the molecular interaction, the greater the increase in the collision cross section due to precession and hence the larger the decrease in the transport coefficients. Further, it was reasonably assumed that the approach to saturation depended upon $\omega_L \tau$, but since ω_L is proportional to H and τ is inversely proportional to the pressure, p, of the gas, it was deduced that the approach to saturation depended upon H/p. All these conclusions are borne out by experimental observations.

This simple theory, though useful in helping us to understand the physics of the phenomenon, has been replaced by more sophisticated theories. This is due to its inability to explain the following experimentally observed facts:

a) The heat conductivity effect at saturation is about twice as large as the viscosity effect at saturation.

b) The change in heat conductivity and viscosity do not have the same dependence on the magnetic field.

c) The field gives rise to a transverse heat flux perpendicular to the applied temperature gradient through the gas, and also to the applied field.

Also, the theory does not work for rough spherical molecules such as methane. Finally, it may be said that though the

theory was proposed only to explain the behaviour of paramagnetic molecules, it may be immediately extended to diamagnetic molecules.

A more fundamental description of the transport phenomena has emerged through the contributions of various researchers [13-23], [25]. It has been shown independently by Waldman[14] and Kagan and Maksimov[13] that when a temperature gradient is impressed on a gas, it produces anisotropy not only in the velocity distribution but also in the angular momentum distribution of the gas. Dahler, et.al.,[16-20] have calculated the influence of the anisotropies on the transport properties of loaded spherical and rough spherical molecules. (The collisional mechanics of rough spheres and loaded spheres is extensively discussed by Chapman and Cowling[24].)

In the presence of a magnetic field, the precession of the magnetic moment vector gives rise to an extra averaging which tends to destroy the anisotropy in the angular momentum space. This destruction couples back to the destruction of the anisotropy in the velocity space which in turn gives rise to a decrease of the transport coefficients. The modern viewpoint is to look at the extent to which the different types of allowable polarization (in the velocity and angular momentum spaces and their various combinations) are destroyed by the field[25]. The Kagan vector, $(\overline{C}\cdot\overline{J})\overline{J}$, and the Waldman vector, $\overline{C} \times \overline{J}$, are two such polarizations; where $\overline{C}$ is the reduced

thermal velocity and $\bar{J}$ is the reduced angular momentum.

Kagan and Afanas'ev[15] were the first to solve the Boltzman equation by using the Chapman-Enskog method. In their model, the molecules were assumed to be non-spherical, but their collisions were taken to be elastic, i.e., the angular momentum vector was assumed to remain invarient through the collisions. Kagan and Maksimov[13] extended the work to include the presence of magnetic fields. Beenakker, et.al.[4, 25] not only applied the theory to include diamagnetic gases, but also extended it to include off-diagonal terms of the thermal conductivity matrix and the viscosity tensor. (See Appendix A for a detailed discussion of the thermal conductivity matrix.) In fact, it is clear now, that the magnetic moment of a molecule serves merely as a "handle" to make the molecules precess, but does not in any way determine the magnitude of the magnetic effect at saturation. This depends only upon the non-sphericity. Experimental data have proven the above conclusion to be true[11][27]. Thus, though the magnetic moment is about a thousand times larger for oxygen than it is for nitrogen, the magnitude of the S-B effect at saturation is about equal for both the gases. But of course, it takes a much higher field to cause nitrogen molecules to precess fast enough to cause the effect to saturate[12].

In recent times, progress has been made too in including the effects of inelastic collisions. Starting with the

Waldman-Snider equation, McCourt and Snider[23] have given a treatment which does exactly that. Meanwhile, Waldman and Hess[27] used Grad's moment method to study the quantum mechanical version of an "energetically elastic" collision model which includes reorientation effects. That is to say, they allowed the direction of the angular momentum vector to vary, but not its magnitude--no energy transfer being allowed between the rotational and translational kinetic energy of the colliding molecules. Kagan and Maksimov have also devised a method of accounting for inelastic collisions by treating the non-sphericity of the molecules as a perturbation on a dominant spherical part.

The elastic collision model based theories give a good phenomenological description of the observed effects and also the correct H/p dependence for the thermal conductivity. However in the case of viscosity, due to a much larger proportion of inelastic collisions, the agreement between theory and experiment is rather poor. To remedy this, Korving, et.al.,[58] following the method of McCourt[22], have obtained the correction factors necessary to account for the inelastic contributions. It may be noted that in the case of thermal conductivity, although the inclusion of inelastic collisions does not change the field dependence, it does influence the magnitude of the S-B effect, since heat energy is then transferred both by rotational and translational degrees of freedom.

THEORETICAL RESULTS

Knapp, et.al.[25] solved the linearized Boltzmann equation by the Chapman-Enskog method for elastic collisions. Retaining only the Kagan vector polarization term, they obtained:

$$\left(\frac{k_H - k_o}{k_o}\right)'' = \frac{\delta k''}{k} = -2\psi\left(\frac{\theta^2}{1+\theta^2}\right)$$ Magnetic field parallel to applied temperature gradient

$$\left(\frac{k_H - k_o}{k_o}\right)^{\perp} = \frac{\delta k^{\perp}}{k} = -\psi\left(\frac{\theta^2}{1+\theta^2} + 2\,\frac{4\theta^2}{1+4\theta^2}\right)$$ Field perpendicular to gradient

$$\left(\frac{k_H - k_o}{k_o}\right)^{T} = \frac{\delta k^{T}}{k} = -\psi\left(\frac{\theta}{1+\theta^2} + 2\,\frac{2\theta}{1+4\theta^2}\right)$$ Heat flux perpendicular to both the field and the temperature gradient

where k_H = thermal conductivity of the gas in the presence of field H,

k_o = thermal conductivity of the gas in zero field,

$$\psi = \frac{6}{125}\beta^2\left(1 - \frac{3}{4}\frac{\Omega^{21}}{\Omega^{11}}\right)^2\left\{1 + \frac{25}{4}\frac{\Omega^{11}}{\Omega^{22}}\left[1 - \frac{4}{25}\beta^2\left(1 - \frac{3}{4}\frac{\Omega^{21}}{\Omega^{11}}\right)^2\right]\right\}^{-1}$$

$$\theta = \frac{3}{8\sqrt{\pi}}\left(\frac{g_L\,\mu_N\sqrt{kT\,m}}{\hbar\,\sigma^2\,\Omega^{(1,1)}}\right)\frac{H}{p} = R\left[\frac{H}{p}\right]$$

β = non-sphericity parameter

Ω^{11}, Ω^{21}, Ω^{22} are Omega integrals[30]

$$\Omega^{(1,1)} = \left(\frac{\Omega^{11}}{\Omega^{11}_{HS}}\right)$$

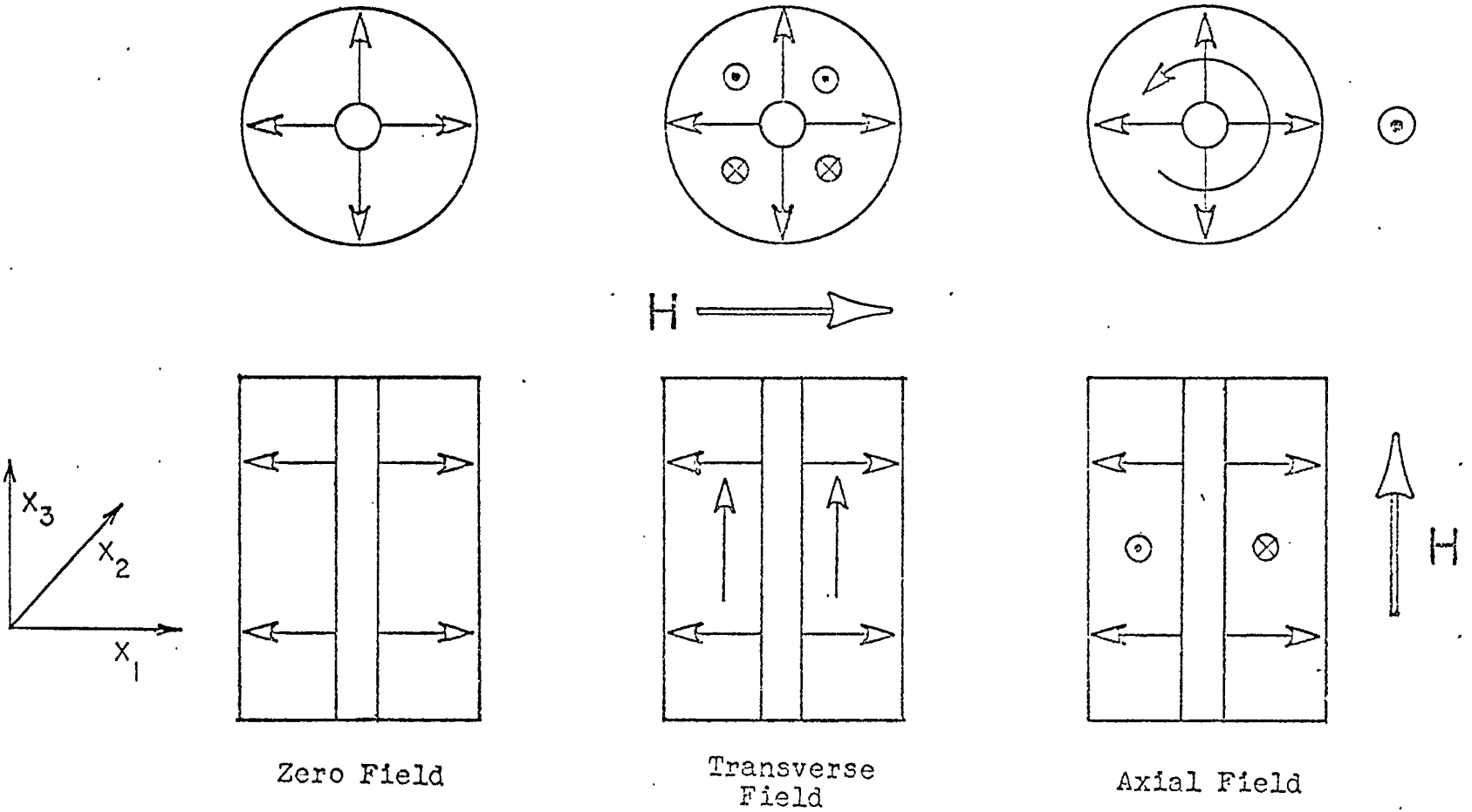

Figure 2: Heat Transfer in the Cell With and Without the Field

Ω^{11}_{HS} = Omega integral for a hard sphere

$= \sigma^2 \sqrt{\frac{\pi kT}{m}}$

g_L = Lande' g-factor

μ_N = nuclear magneton

T = absolute temperature

m = mass of the gas molecule

$\hbar$ = Planck's constant

σ = hard sphere diameter

Note that $\delta k^{\parallel}/k$ and $\delta k^{\perp}/k$ are even in H, while $\delta k^{T}/k$ is odd in H. Also, as H/p tends to infinity,

$\frac{\delta k^{\parallel}}{k}$ approaches $- 2\psi$

$\frac{\delta k^{\perp}}{k}$ approaches $- 3\psi$

$\frac{\delta k^{T}}{k}$ approaches zero.

The observed data fit the above equations so well (using ψ and R as adjustable parameters) that it is difficult to determine the effect of other polarizations[25].

Finally, it may be noted that θ may be written as $\omega_L \tau_C$ where τ_C is a characteristic time for the collision process, and in general is considerably larger than the time between two elastic collisions. On making this substitution, the equations so obtained resemble very much the one expressing the response of a system with a relaxation time τ to a periodic disturbance of frequency ω. In this light, τ_C may be considered

to be a "characteristic relaxation time" of the gas involving the reorientation time of the angular momentum. In fact, it may easily be shown that the expressions for $\delta k^{\perp}/k$ and $\delta k^{T}/k$ obey the celebrated Kramers-Kronig absorbtion-dispersion relationships. Calculations of τ_c based on Senftleben measurements agree remarkably well with that obtained from NMR work (31).

CHAPTER II

DESIGN CONSIDERATIONS AND DESCRIPTION OF THE EXPERIMENTAL APPARATUS

GENERAL DESIGN CONSIDERATIONS

Undoubtedly, the most important design consideration is the magnitude of the S-B effect. It is known from previous experiments[5-7][32] that the change in thermal conductivity for oxygen even at saturation is about one percent. The effect is even smaller for other gases. Hence the apparatus must have a resolution of 10^{-6} in $\delta k/k$ or better. Since it is virtually impossible to make absolute measurements with this degree of accuracy, it was decided to construct a differential type of apparatus.

Typically, a thermal conductivity apparatus consists of a volume full of the gas under study, the boundaries of which are maintained at different temperatures by a constant heat flux. Any change in the thermal conductivity of the gas would bring about a change in the temperature gradient across the gas, and hence a change in the temperatures of the boundaries. Ideally, in a differential apparatus, one would like the steady state temperature of one of the walls to remain absolutely constant. Also, one would like to be able to use a temperature sensor that is unaffected by magnetic fields to monitor the temperature of the other wall, so that, the entire perturbation

sensed by it when the magnetic field is switched on may be attributed to the S-B effect.

It was with these objectives in mind that a low temperature probe was constructed to be used with the Magnion 100,000 gauss superconducting magnet. This solenoid has an effective cylindrical working volume 3" long and 1.5" in diameter. The probe was installed in the magnet and the system cooled down to the operating temperature range viz. $77^{o}K$ - $100^{o}K$. The temperature drift rates and control were found to be good, and the measured thermal conductivity of nitrogen and helium in zero magnetic field agreed to within 5% of the literature values. Heat leaks from the cell were reduced over previous cells by a factor of 3.

The probe, however, failed to display the degree of sensitivity that was expected of it; mainly because of a large magneto-resistance correction to the temperature sensor. (A detailed description of this probe will be presented by the author in a dissertation currently in progress). In order to solve this problem and to gain experience in making S-B effect measurements, it was decided to construct another probe which would be used with the Magnion (Model L-96) 16,000 gauss electromagnet which is much easier and much cheaper to operate than the superconducting one.

The additional broad design considerations for the probe were:

a) it should be simple and yet flexible enough to take a lot of modifications, if the need arose,

b) it should be operable in a wide temperature range of $20^{\circ}K$ to $300^{\circ}K$,

c) it should fit both the magnets so that data taken on both parallel and perpendicular effects and possibly even transverse effect, and

d) it should be possible to use it to obtain magneto-resistance data for several temperature sensors, to calibrate thermistors against a pre-calibrated platinum resistance thermometer and to calibrate field sensing devices such as Bismuth "Mistor" elements.

CELL DESIGN

An "infinite" concentric cylinder type of cell was chosen over other geometries because such cells have lower heat leaks, are easy to make and seem to be a natural choice for the cylindrical superconducting solonoid. Also, radiation corrections are easy to make. A parallel plate type cell does, however, have its advantages. For while the cylindrical cell would require the use of both the superconducting magnet and the electromagnet to measure $\delta k^{\perp}/k$ and $\delta k^{(\perp + \parallel)/2}/k$, from which $\delta k^{\perp}/k$ and $\delta k^{\parallel}/k$ may be back calculated; these quantities may be directly measured in the electromagnet by merely rotating the probe by 90°. (See Appendix A for proof.)

A concentric cylindrical cell, a drawing of which appears

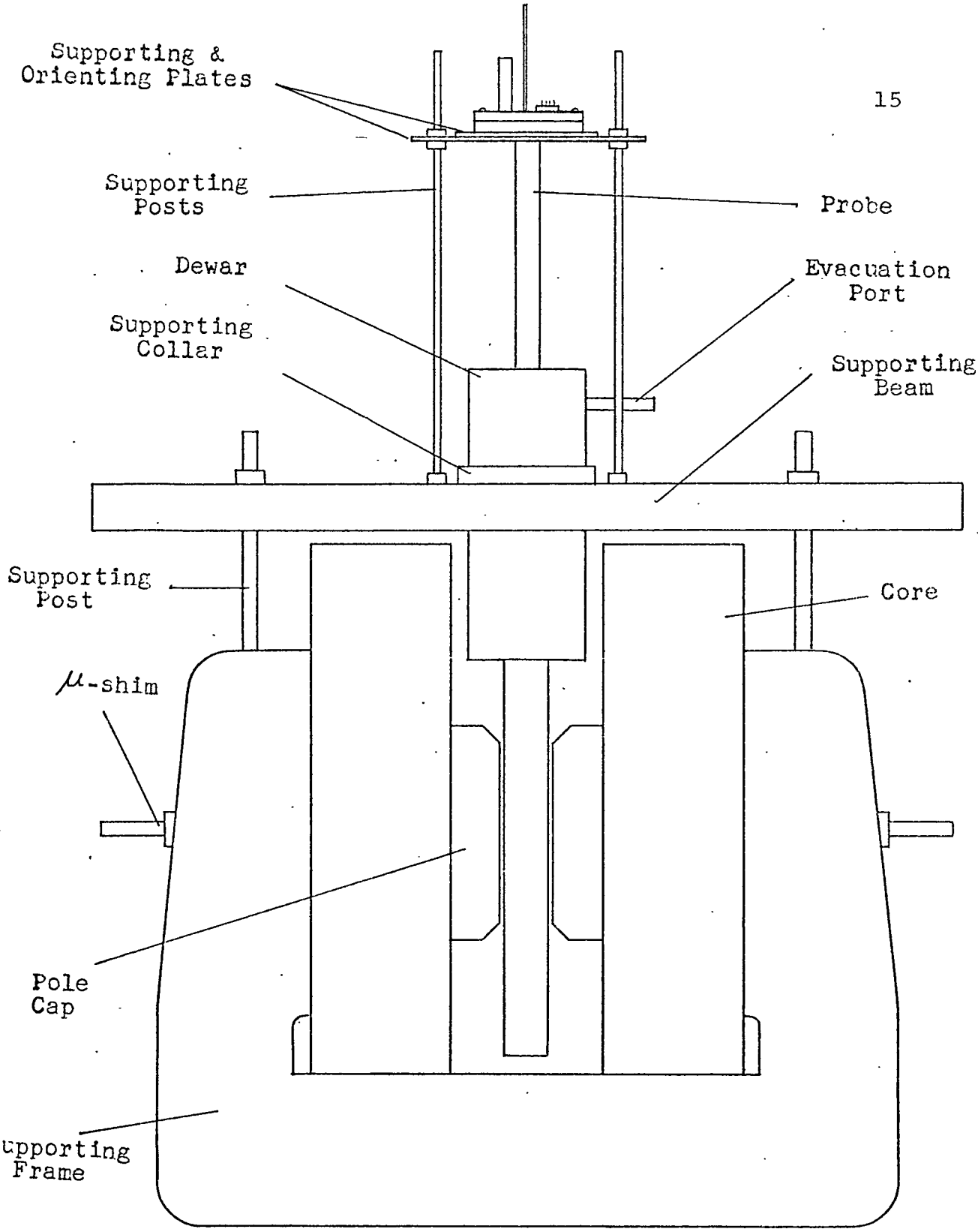

Figure 3: The Experimental Apparatus

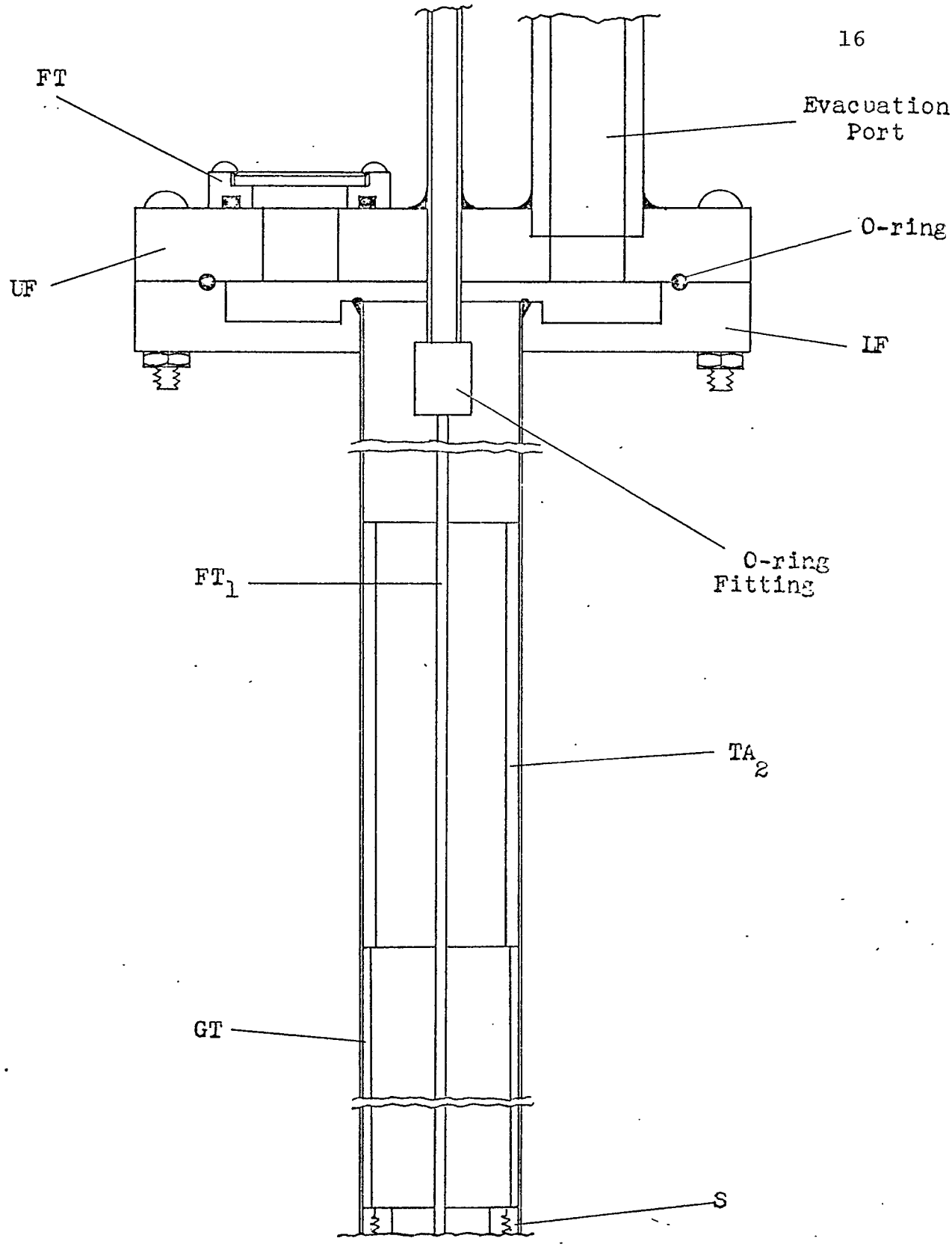

Figure 4a: Longitudinal Section Through the Top Part of the Probe

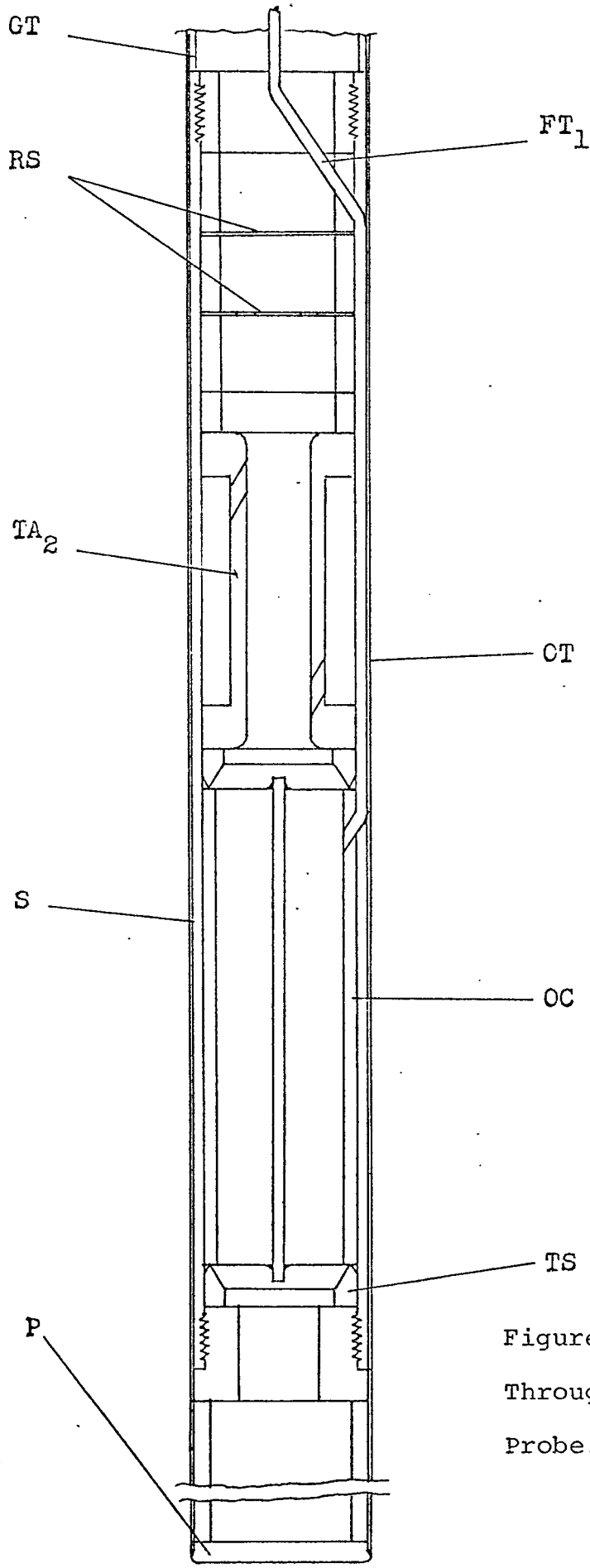

Figure 4b: Longitudinal Section Through the Bottom Part of the Probe. (Overall Length: 36½ inches)

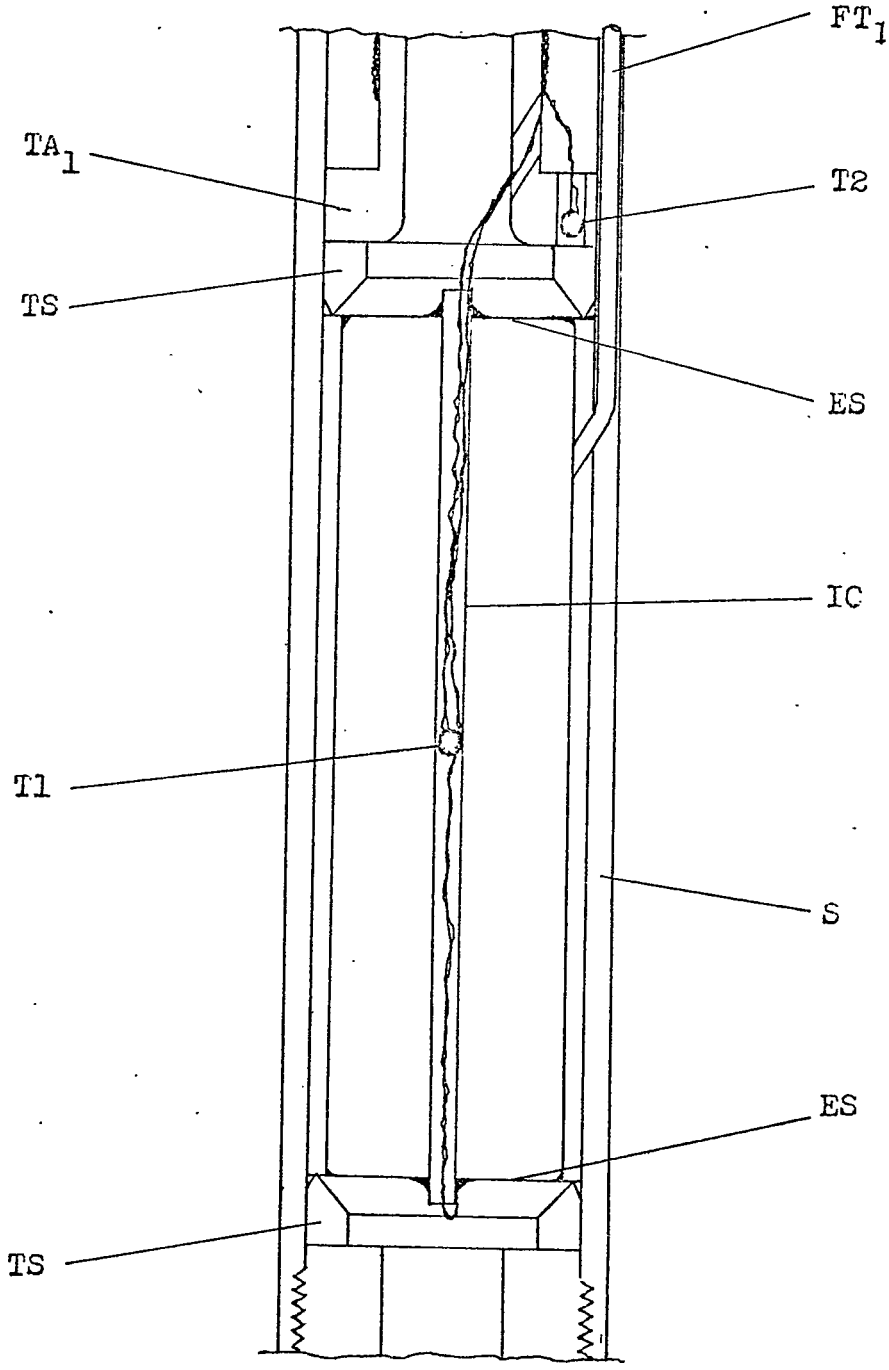

Figure 5: Details of the Cell in Section

in Figure 5, was therefore used. The outer cylinder (OC) was made relatively massive and placed in intimate thermal contact with a brass sleeve (S) in order to give it a large thermal mass and enhance heat dissipation. The inner cylinder (IC) by contrast was made with a minimum mass of material as possible. Now, with constant heat flux from the IC to the OC, any change in the thermal conductivity of the gas in the cell would produce a change in the driving force, ΔT, between the IC and the OC. However, the temperature of the OC is held constant by virtue of its good dissipation and large thermal mass; as a result, the temperature of the IC will change to reflect the change in the thermal conductivity of the gas. Hence, monitoring the change in the temperature of the IC with respect to the OC provides a good differential technique.

The length of the cell was limited to 3 inches by the working space available in the superconducting magnet. The outer diameter of the OC was fixed by the I.D. of the dewar to be used between the poles of the electromagnet. The wall thickness of the OC was made large enough to minimize any axial thermal gradients along it, and for the same reason it was made out of oxygen free high conductivity copper.

The diameter of the IC was a little more difficult to design because several competing factors were to be considered. Firstly, since the S-B effect varies as H/p, it appears desirable to work at low pressures. However, the pressure cannot

be reduced indefinately, because as the pressure is decreased, the mean free path length of the gas molecules increases (at constant temperature) as shown in Figure 6. The consequence of which is that the anomalous Knudsen effects increase so that the simple steady state heat conduction equations no longer hold[33][34]. Larger diameter inside cylinders help reduce the Knudsen effects and therefore permit operation at lower pressures. Secondly, the IC diameter must be large enough to permit a sensor to be placed on the inside of it. On the other hand, if the diameter is increased for a given wall thickness, the mass of the IC increases and so does its time constant. Also, thin walled large diameter tubes collapse under smaller pressure differentials, and they are difficult to make. After due consideration to all these opposing factors, a compromise diameter of 0.13 inches was decided upon. Calculations show that, at a pressure of 1 torr., the cell would still be well within the continuum regime. (See Chapter V for details.)

The end seals (ES) connecting the two cylinders were made out of thin Mylar sheets. Mylar was chosen because it can be obtained in thin sheets, has low gas diffusion rates, has high tensile strength even at low temperatures, and has a low thermal conductivity which comes to within an order of magnitude of most gasses at low temperatures.

DESIGN OF THE REST OF THE PROBE

The rest of the components of the probe were, so to say, designed around the cell. Their functions were to support the cell between the poles of the magnet, add to the thermal mass of the outer cylinder of the cell, keep it thermally isolated from the surroundings, and provide a high vacuum environment on the outside of the cell. Vacuum "feed throughs" (FT) were designed for the electrical leads and the cell filling tube to pass from the evacuated part of the probe to the electrical measuring apparatus and the filling system respectively.

All metallic components were made from non-magnetic metals and alloys. Whenever high thermal conductivity was necessary, Oxygen Free High Conductivity (OFHC) copper was used; for example, in the OC of the cell and the thermal anchors (TA_1 and TA_2). But when good machining properties were deemed important enough to justify some sacrifice in thermal conductivity, ordinary "yellow" brass was used; for example the sleeve S. However, when thermal insulation was a prime requirement, Type 304 or 321 stainless steel was used; for example, the outer skin of the probe. Brass was used for all other parts. It may be remarked that all the metals used were easily bonded by either soft soldering or silver soldering.

All permanent metal to metal joints were soft soldered. Mylar film to metal joints were made with Goodyear G-207

polyester resin and catalyst mixture. No special surface treatment was required aside from mechanical and solvent cleaning of the surfaces joined. Both the above mentioned techniques worked remarkably well even under rapid thermal cycling. All room temperature seals that needed to be dismantled frequently were made with "Viton" O-rings of the appropriate size.

DESCRIPTION OF THE CELL

The cell consisted of two coaxial cylinders. The outer one (OC) was machined to the size shown in Figure 5 from a rod of OFHC copper. A 1/16 inch O.D., type 321, stainless steel tubing of appropriate length was soldered obliquely through the wall to serve as a sample gas filling tube. The inner cylinder (IC) was made by wrapping a rectangular piece of 1 mil aluminum foil of suitable dimensions on a 0.120 inch diameter rod and then slipping it carefully off to give a cylinder 3.2 inches long, with a wall thickness of 0.004 inch. To make sure that no gasses would leak through the cylinder, a creaseless piece of foil was used, and both sides of the foil were greased with Apiezon High Vacuum Grease (Type N) before wrapping. As an added precaution, a thin layer of General Electric Adhesive No. 7031 was applied on the outside of the cylinder for sealing purposes. The inner cylinder heating element (ICH) consisted of a 14 inch length of 1 mil Evanohm*wire (with a resistance of 845 Ω/foot) which was

*Trademark of Leeds & Northrup Co.

uniformly and bifilary coiled around the cylinder and thermally anchored to it by an additional layer of the adhesive. Needless to say, such an inner cylinder was large enough to contain a temperature sensor inside it and to reduce Knudsen effects but yet was light enough to have a small time constant of about 2 minutes. A small time constant was important because it allowed quick S-B effect measurements; and hence decreased uncertainty due to temperature drifts. The good thermal conductivity and uniform thickness of the aluminum foil ensured uniform temperature distribution along its length. Many or all of these advantages were not available in previous experimental apparatuses used. The same concept could also be used to make the hotter plate of a parallel plate type of thermal conductivity cell.

The cell assembly was completed by gluing on a pair of 1 mil Mylar discs, one on each end of the cylinders as shown in the figure. They serve as vacuum tight end seals and also help support the IC. Care was taken to use as little glue as possible in order to minimize heat leaks through the seals. After the glue was cured for three days at room temperatures, warm air was blown over the seals to cause them to shrink and hence prevent the IC from sagging due to its weight. This arrangement made the IC almost adiabatic, except for the desired heat transfer through the sample gas.

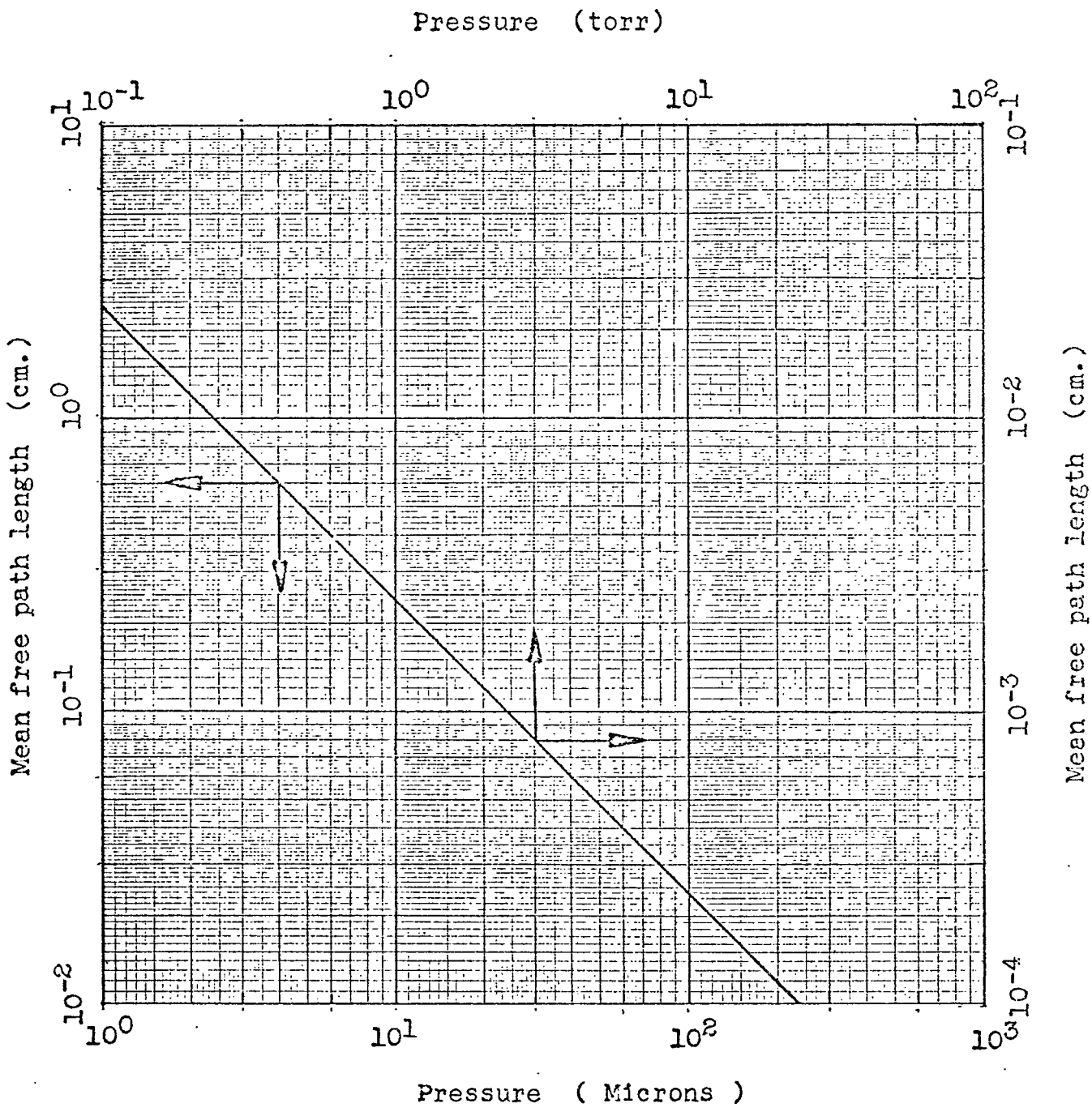

Figure 6: Variation of the Mean Free Path Length for Nitrogen with Pressure at $77.3^{\circ}K$

DESCRIPTION OF THE CELL HOLDER AND SUPPORTS

The cell was placed inside a brass sleeve (S) which was well greased on both the inside the the outside for good thermal contact. The sleeve helped to hold the cell, the thermal anchor (TA_1) and the radiation shields (RS) in place, and added to the thermal mass of the OC.

To insulate the ends of the cell, so as to make it approximate more closely the heat conduction model of a pair of infinitely long concentric cylinders, two teflon spacers (TS) were designed to have only a line contact with the ends of the cell.

The radiation shields were merely thin polished brass discs with two holes drilled in them to enable evacuation of the probe and let the electrical leads pass. The discs were so placed relative to each other so that the cell was not exposed to direct radiation from the warmer parts of the probe.

Electrical leads from the cell were thermally anchored at two points before passing out through the probe header. The upper anchor (TA_2) was 3 inches long and made of brass and the wires were anchored to its inner surface. It served to dissipate most of the heat conducted down along the copper leads to the liquid nitrogen bath. The anchor was isolated from the sleeve, S, by a short length of 1 inch O.D. glass tubing. The second anchor (TA_1) made of OFHC copper complemented the function of the first and brought the leads down

to the temperature of the OC. Thermal anchoring on both anchors was achieved by grease, while mechanical anchoring was obtained by beryllium springs.

All the above mentioned components were supported from above by a thin walled (0.020 inch thick), 1 1/8 inch O.D. type 321 stainless steel tube (OT) with a brass plug (P) soldered at the lower end and two flanges (UF and LF) on the upper end. The flanges were used to support the whole assembly in a dewar (D) containing liquid nitrogen. They also helped to vacuum seal the holder and allowed easy loading and unloading the cell. Also, they provided suitable egress to the electrical leads and the 1/16 inch filling tube, FT_1.

The cryostat consisted of a stainless steel, double walled dewar--evacuated by a high vacuum system--which was filled with liquid nitrogen (or the appropriate coolant). The shape and size of the dewar, the supports for the probe and dewar are made clear in Figure 3. The support for the probe was such that it could be rotated about its axis and clamped in any desired position. (See Figure 4.)

THE HIGH VACUUM SYSTEM AND THE SAMPLE GAS FILLING SYSTEM

The mobile high vacuum system consisted of an air cooled NRC 3 inch oil diffusion pump (Model No. HSA-150) backed up by a Welch Scientific 1402 Duo Seal forepump (see Figure 7). It was used to evacuate the cell, the space outside the cell, the sample gas filling system, and the cryostat dewar. It is

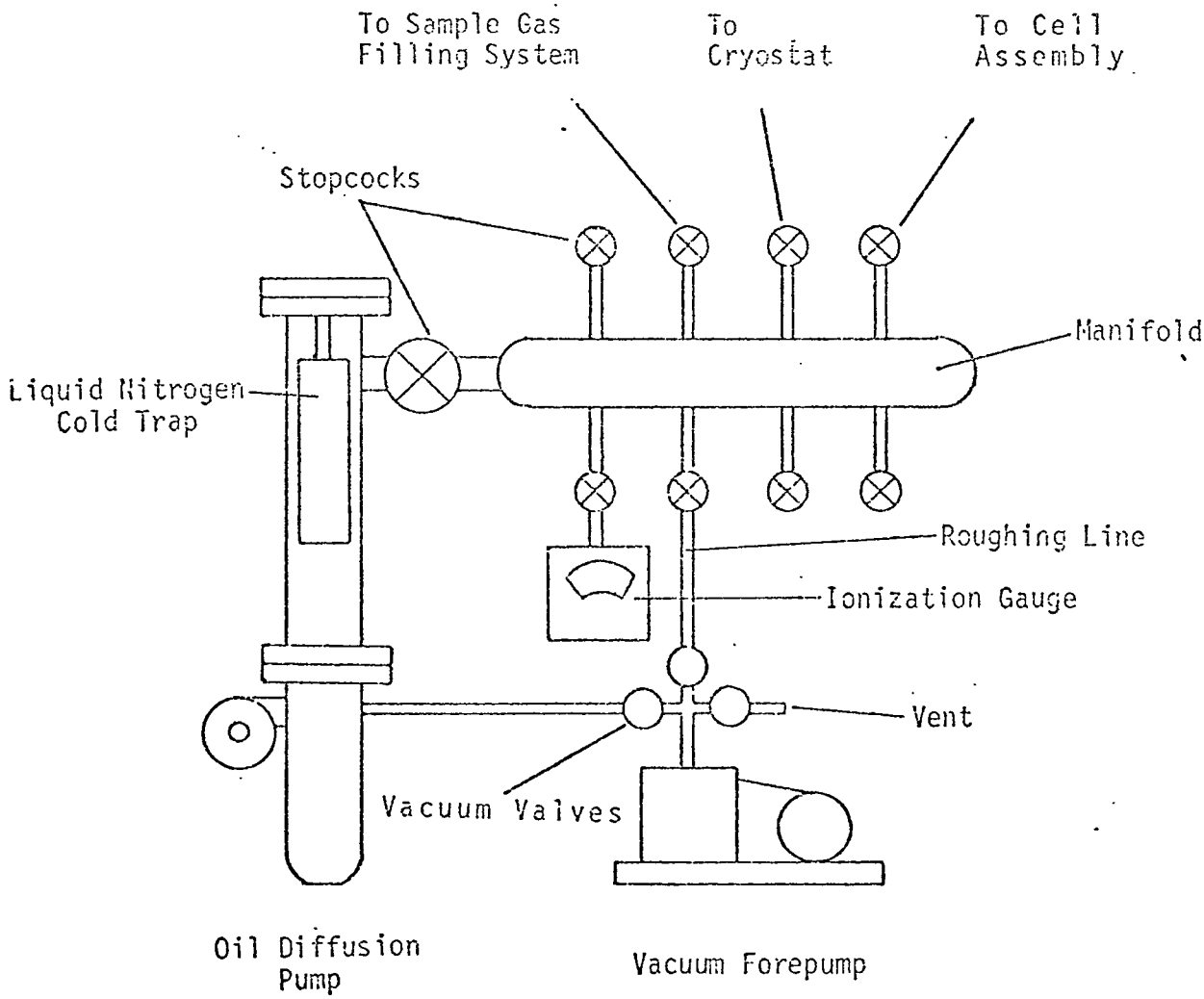

Figure 7: Schematic of the High Vacuum System

capable of attaining a vacuum of 10^{-7} torr. and better and has a pumping speed of 100 liters of air per minute. The performance was improved by a liquid nitrogen cold trap. Connections from the vacuum system to the filling system, probe, etc. were made via 3/4 inch I.D. bronze bellows tubing. A CVC Phillips Gauge (Model No. PHG-09) with a range of 10^{-7} torr. to 0.5 torr. monitored the pressure of the high vacuum system. For a detailed description, the reader is referred to the M.S. Thesis by D. G. Elliot[35].

The filling system was used to evacuate the cell, fill it with the sample gas, and measure its pressure. Essentially it was a maze of 1/4 inch copper tubing and several Nupro (H-Series) valves arranged in a suitable manner, as shown in Figure 8. It was connected through separate valves to a Welch Scientific 1402 Duo Seal mechanical pump for rough pumping and to the high vacuum system for attaining high vacuums. Three gauges were attached to the system: a Crosby, Bourdon tube type of vacuum gauge (range: 0-30 inches of mercury) which was used to monitor the pressure during rough pumping, a Wallace and Tiernan FA-160 absolute pressure gauge (range: 0.1-20 mm of mercury) and a Stokes M-3 absolute pressure thermocouple gauge (range: 1-100 μ). The last two were used to measure the pressure of the sample gas. The system was capable of filling sample gasses from two pressurized gas bottles through two Matheson 2-stage (Model 19) high purity

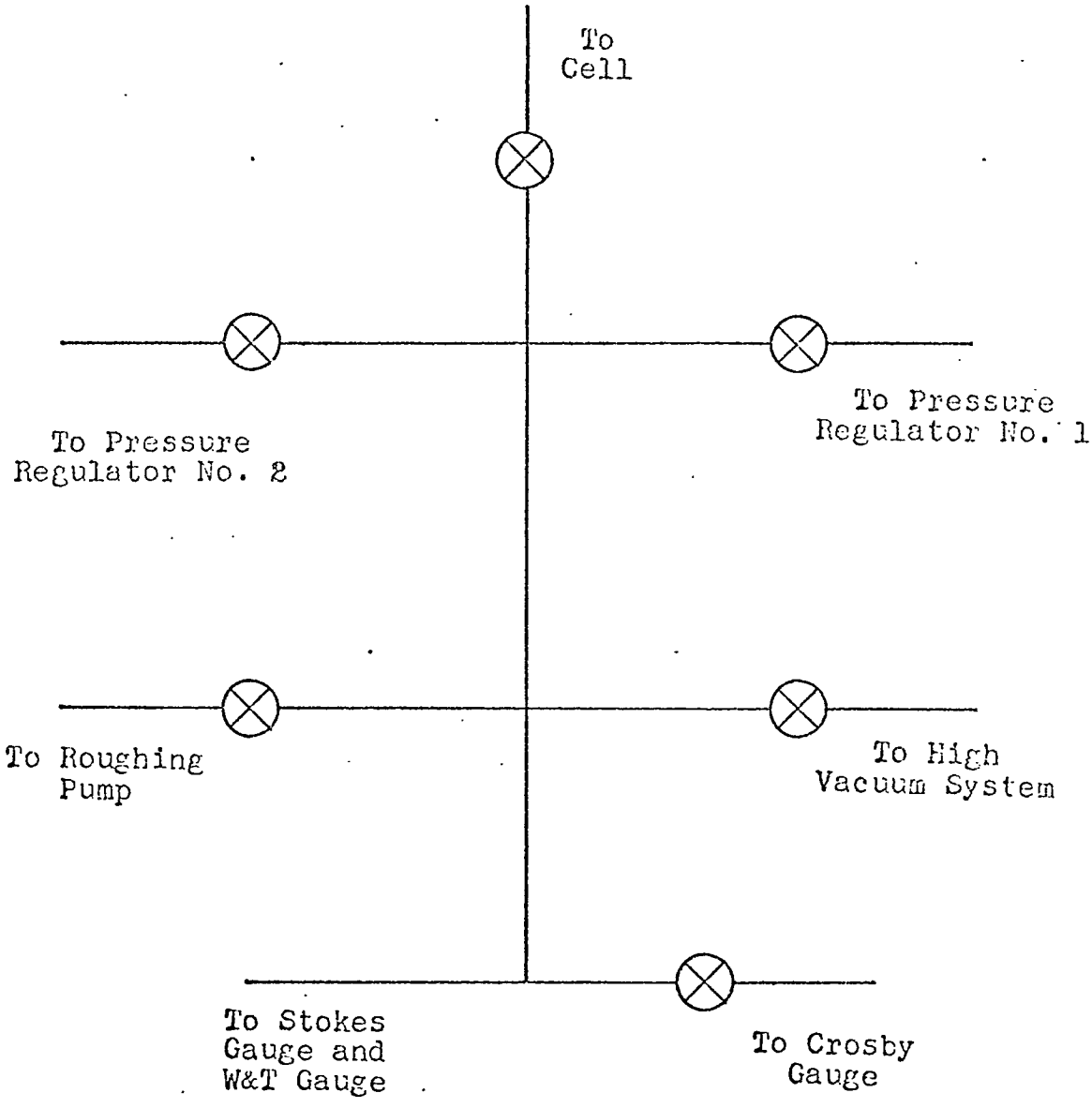

Figure 8: Schematic of the Filling System

regulators. All connections to and within the system were made by Swagelok tube fittings with teflon front ferrules and brass back ferrules for high vacuum operation.

CELL HEATER AND POWER MEASUREMENT CIRCUIT

The circuit diagram for the power supplying and measuring circuits is presented in Figure 9. The conventional four-lead potentiometric method is used to measure the power supplied to the heater (ICH). Four 1.35 volt Mallory mercury cells (Size D), either all connected in parallel, or two sets connected in parallel--each consisting of two cells in series--formed the power supply. The potential drops across the ICH and a standard 10Ω resistor were measured by a Leeds and Northrup Model 7554-K4 potentiometer (range: 0-16.1 volts) connected to a Leeds and Northrup 9834-1 null detector. All the leads and connecting cables were shielded. For further details see reference 35.

CHOICE OF TEMPERATURE SENSOR AND TEMPERATURE MEASURING CIRCUITS

It was decided to use negative temperature coefficient, low temperature thermistors over other types of temperature sensors. Their small size, and hence small time constants, high sensitivity and convenience in use help tip the scales in their favor. A good survey of various temperature sensors and the justification as to their selection is found in reference 36. However an important factor, the influence of magnetic fields on the sensor, was not given its due in the

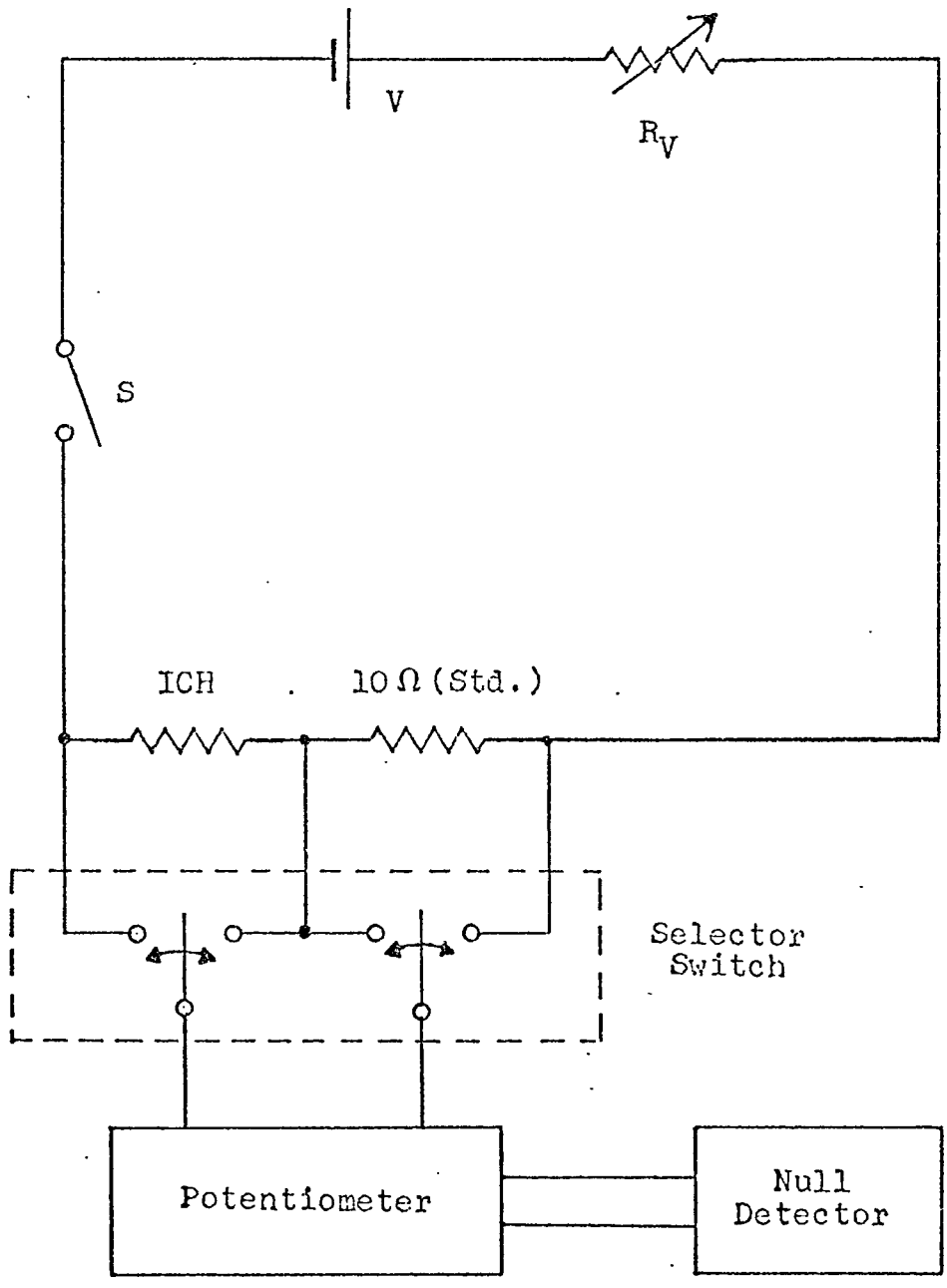

Figure 9: The Heater Power Supply and Measuring Circuit

initial choice. After large field effects were discovered[36], the author undertook a study of the effect of magnetic fields on various thermoelectric temperature sensors, the results of which are presented in Chapter IV. It was found in fact that these thermistors were affected by magnetic fields to a much larger extent than were the other sensors. These types of thermistors have another major drawback; they have unusually large temperature cycling and/or ageing effects. Finally, thermistors usually have a rather restricted range of applicability. Nevertheless, Keystone Carbon (Type RL 10X04-10K-315-S5) thermistors were used for the S-B effect measurements presented in this thesis. This was made possible by using two closely matched thermistors situated in approximately the same field in opposite arms of the Wheatstone bridge. One thermistor (T1) was mounted on the inside of the IC and the other (T2) in the lower part of TA_1 as shown in Figure 5. The effect was thereby reduced but was not small enough for accurate S-B measurements. A procedure described in the next chapter was therefore devised to make the magnetoresistance effect essentially zero.

With regard to thermal cycling and ageing, it was found that after long use, the original calibration stopped drifting; hence, a couple of "aged" thermistors were used in the experiments. For "unaged" thermistors, in situ calibration would have been necessary for each run. The calibration curve for

the thermistor mounted on the inside of the IC is presented in Figure 10. See Appendix C for thermistor calibration. For use in calculations, Figure 11 gives a plot of the slope of the calibration curve versus temperature.

A schematic of the temperature measuring circuit is shown in Figure 12. With a slight modification, the same circuit was used to make S-B effect measurements. All lead wires were twisted to reduce magnetic induction disturbances, and shielded to reduce noise. The unbalance voltage was detected by a Keithley 147 D.C. Electronic Null Detector (ranges: 30 nanovolts full scale to 100 millivolts full scale, accuracy: 2% of full scale). The output of the null detector was displayed on a Houston Instruments' Omnographic 6520 Recorder (with an Analog Adapter No. 6800 coupled to it). A twin-T filter was used between the detector and the recorder to filter out a cyclic 4.5 Hz. noise which was produced by the interaction of the chopper of the detector and the line frequency. Checks were made to determine the effect of the magnetic field on the null detector, the filter and the recorder. None were found.

DESCRIPTION OF THE MAGNET, POWER SUPPLY AND OTHER ACCESSORIES

A Magnion L-96 Laboratory Electromagnet was used in making the measurements. A pair of foil wound, water cooled copper coils form the pole cores. The pole caps have a diameter

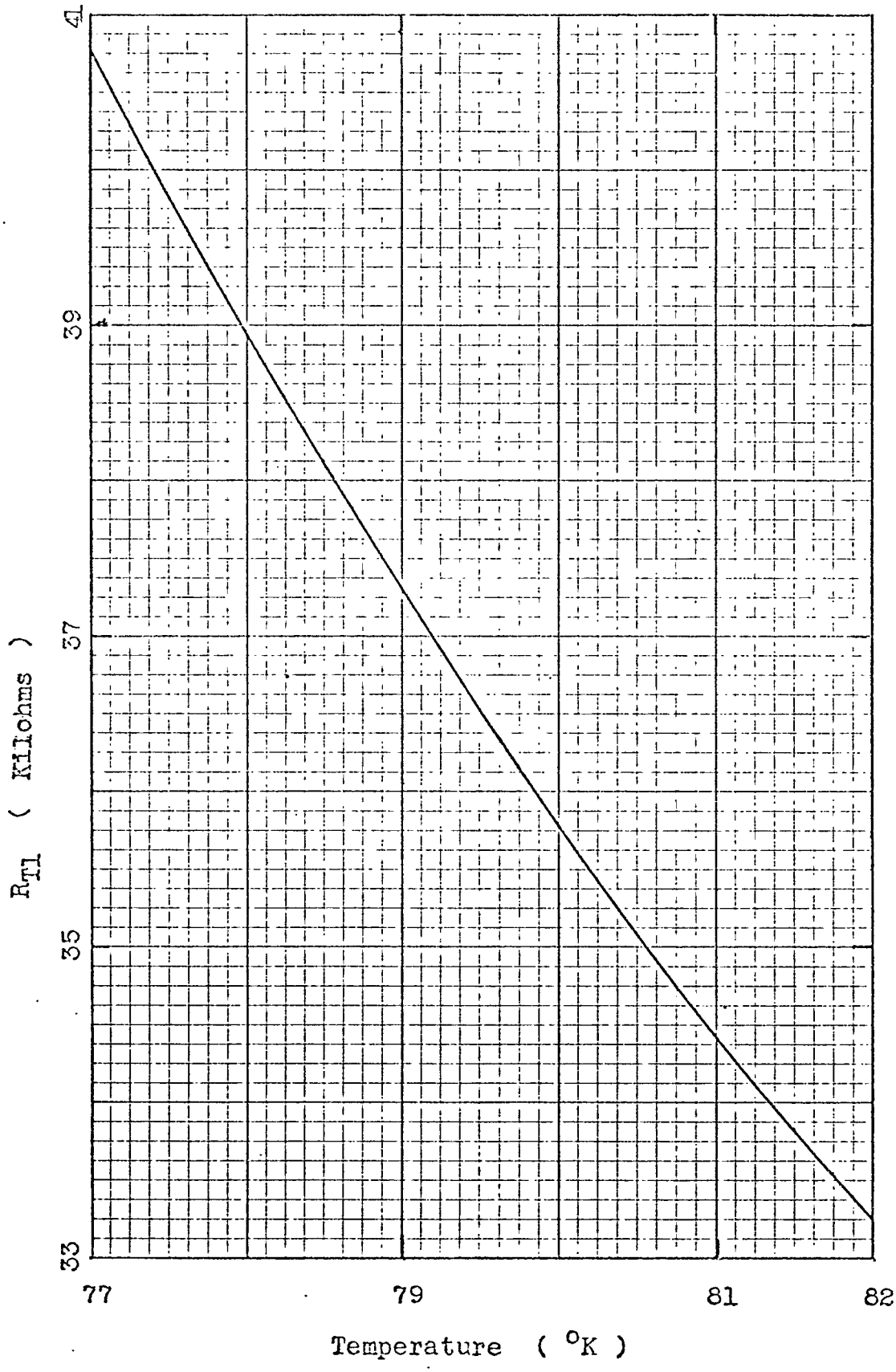

Figure 10: Calibration Curve for Thermistor T1

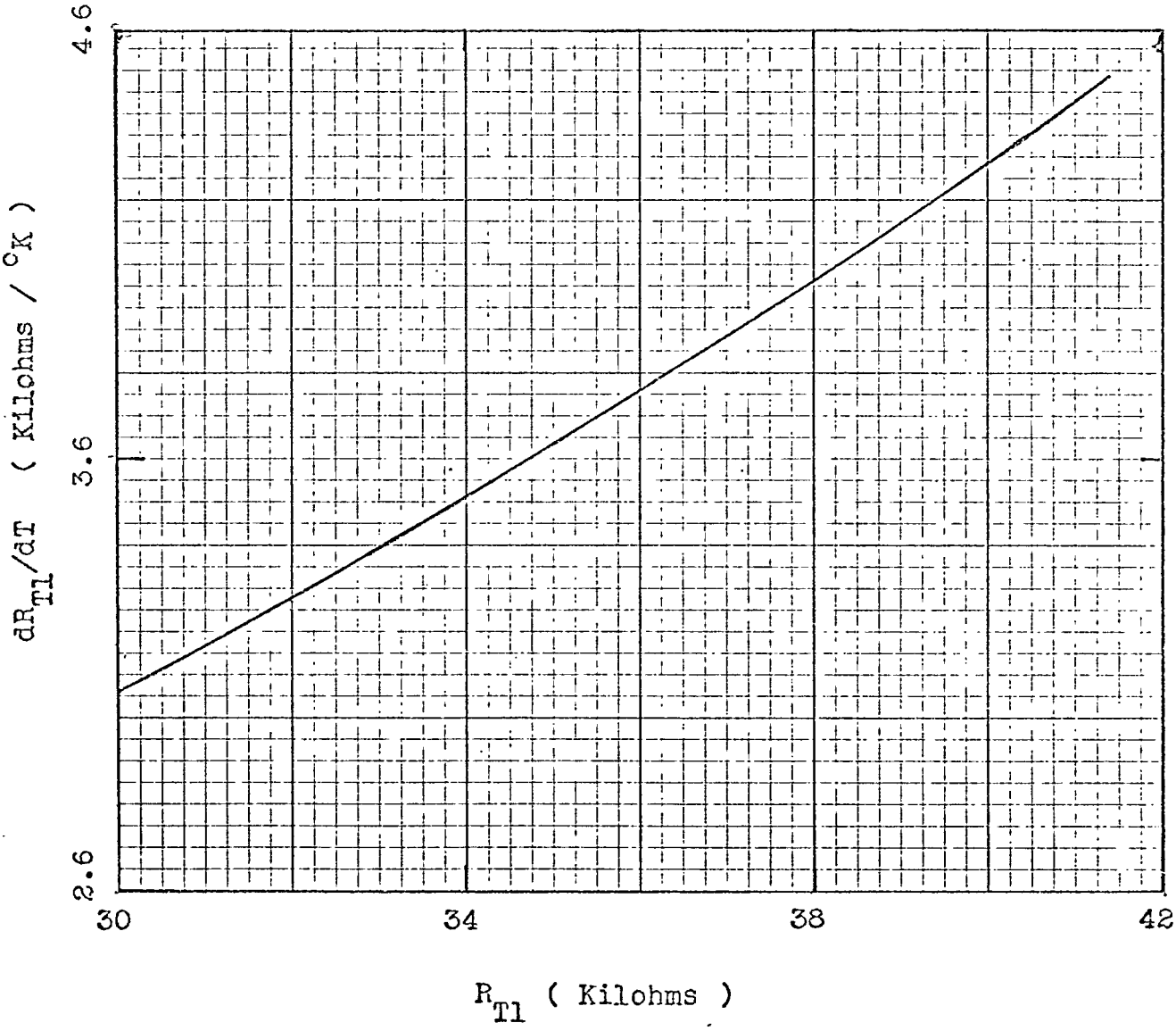

Figure 11: Slope of the Thermistor Calibration Curve Versus Temperature

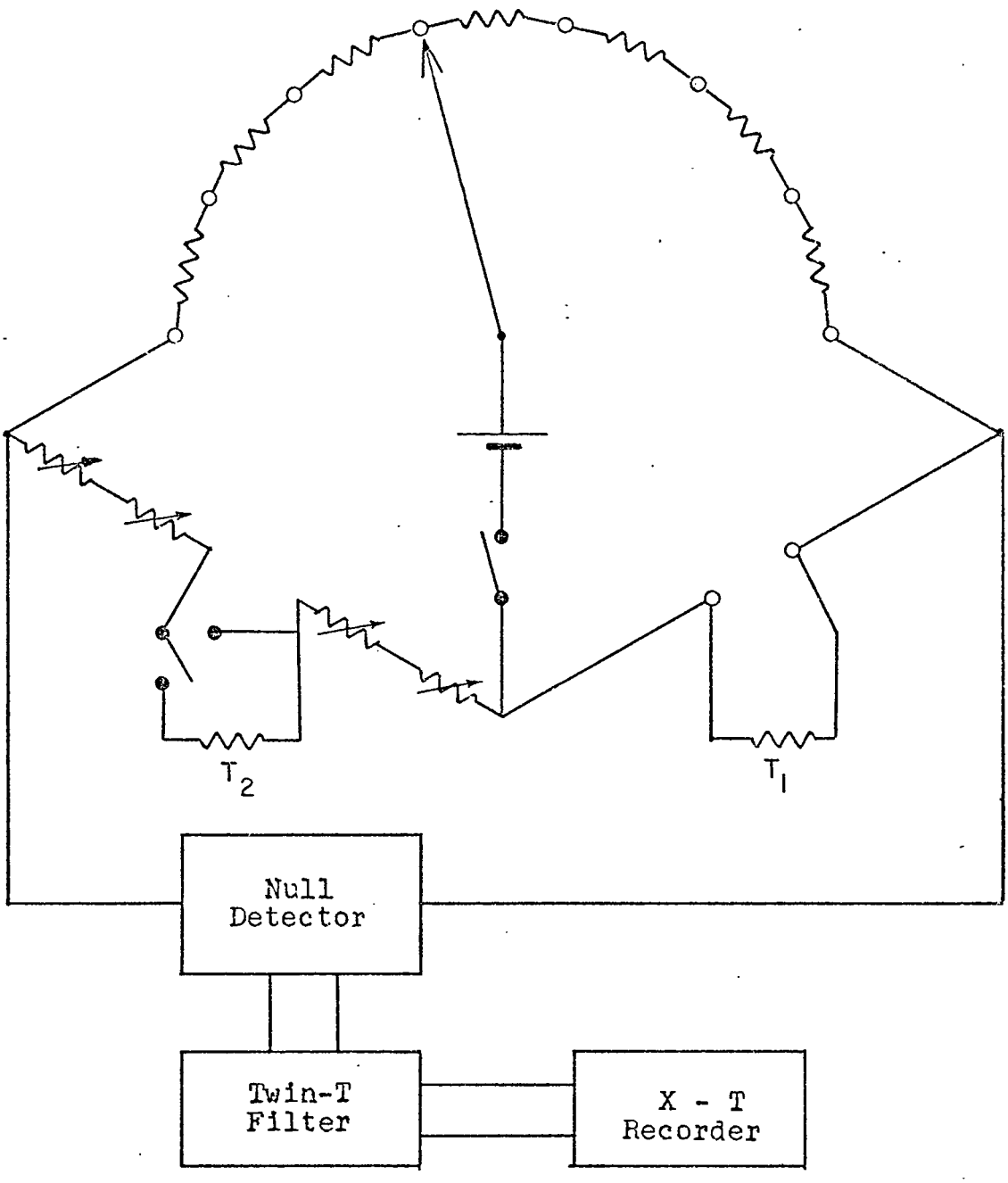

Figure 12: Temperature Measuring Circuit

of 9 inches, tapered to a diameter of 7.5 inches and set at an air gap of 2 inches. A plot of the field homogeneity appears in Figure 13.

The magnet was energised by a Magnion model HS-1265B power supply unit which provided a continuously variable direct current from 0.1 amps. to 65 amps. at 130 volts across a 2Ω load. The stability of the power supply was of the order of 1 part in 10^5 for an 8-hour period.

A closed loop cooling water system which exchanged heat with chilled water at 52^{o}F provided cooling for the magnet cores. A flow switch was installed on the cooling water inlet to the magnet, so that whenever the water pressure fell below 20 psig, the switch de-energised the magnet and thus protected it from damage due to over heating.

SOME SPECIAL PROBLEMS

The rather extreme environment encountered in the experiment such as low temperatures, high vacuum and high magnetic field give rise to some unexpected problems. These will now be aired and the way in which they were solved or circumvented discussed.

Firstly, the thermal conductivity of metals changes with the applied magnetic field. Such a change results in a change of the rate of heat dissipation of the probe to the liquid nitrogen bath and hence in a change in the temperature of the

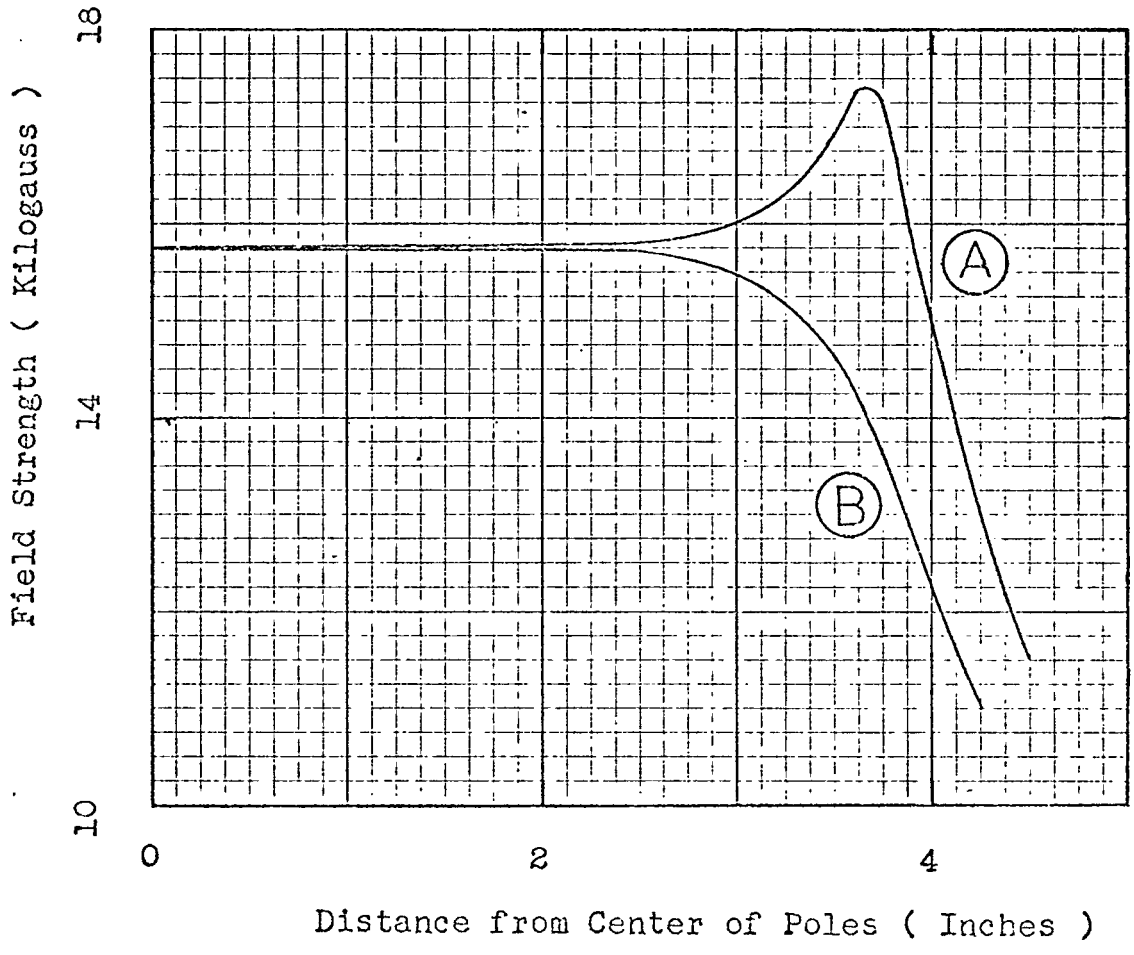

Figure 13: Homogeneity Plot for the Electromagnet

outer cell wall. This problem was solved by making the probe massive and therefore have a large time constant. A more serious consequence was the change in the heat leak to the cell via the heater and thermistor leads due to the field. This was reduced by using two thermal anchors. Both the effects were completely accounted for by repeating the experiment with a noble gas.

The boiling points of liquids are also affected by fields [37]; and since boiling liquid nitrogen forms our heat sink, this effect would produce perturbations in the outer cell wall temperature. The effect was combatted against by increasing the thermal mass of the system.

Another serious difficulty was presented by the fact that the electrical resistivity of electrical conductors is affected by magnetic fields. Hence the resistance of copper conductors, thermistors, and platinum resistance thermometers is strongly affected by fields--a fact borne out by experiment (see Chapter IV). Consequently, automatic temperature control would be unreliable, especially if the temperature sensor was subjected to any significant fields. However, if to avoid this problem, the sensor was physically located far away from the point at which control was desired, i.e., the outer cell wall, the field dependent change in the thermal conductivity of the materials used in making the probe would have made things unpleasant again. The data was therefore taken at a steady temperature drift

rather than at an uncertain "controlled" temperature. The problem was partially solved by using two "matched" thermistors in opposite arms of the bridge as was discussed earlier and by making measurements on a noble gas such as argon.

High magnetic fields can exert strong Lorentz forces on current carring conductors, and hence can cause them to move. Even the slightest movement could produce a perturbation in the temperature indicated by the sensor which could be as large or larger than the perturbation caused by the S-B effect. Such a possibility was forestalled by physically anchoring the thermistors and lead wires firmly in place with glue.

A final problem involved the selection and operation of the bridge. Calculations showed that some of the commercially available bridges, if used without modification, would pass large enough currents through the sensor so that the joule heating of the sensor could be comparable to the heat input of the inner cylinder heater. Proper care was therefore exercised in the selection and use of the measuring bridge.

CHAPTER III

EXPERIMENTAL PROCEDURES

GENERAL REMARKS

As was mentioned earlier, one would like to be able to make Senftleben-Beenakker effect measurements with the steady state temperature of the apparatus, particularly the cell, remaining constant. However, since the probe used to make the measurements had no means of controlling the temperature, all the data presented in this work were taken at a slow and steady temperature drift. The rate of drift was determined by the rate of decline of the level of liquid nitrogen in the cryostat. The effect of the drift was, to some extent, reduced by measuring the temperature of the inner cylinder (IC) relative to that of the outer one (OC), while both were steadily drifting; hence permitting the use of more sensitive scales on the detecting and recording equipment.

The minuteness of the effect measured, the complexity of the apparatus, and the extreme environment of the cell would in general leave a lot of room for spurious effects to creep in. To make sure that these were eliminated (or accounted for), the experiment was repeated under identical conditions with argon as the sample gas. Being a monatomic gas, argon experiences no perturbation of its transport properties when subjected to magnetic fields.

SETTING UP AND TESTING THE EQUIPMENT

The thermal conductivity cell was constructed as shown in Figure 5, care being exercised to keep the inner surfaces of the various components as clean as possible. This precaution was essential to avoid contamination of the sample gas. The finished cell was then placed in a specially built evacuation chamber for leak testing. The air on both the inside and the outside of the cell was pumped out. The evacuation was done gradually to avoid subjecting the end seals and the delicate inner cylinder to too large a pressure differential. Ultimately a vacuum of 10^{-6} to 10^{-7} torr. was obtained. The cell was usually pumped on for a couple of days more to permit the glue solvent, fingerprints, etc. to outgas.

The cell was then pressurized to a pressure of 15 torr. by filling it with helium. If while the cell was being filled the pressure on the outside of the cell remained unchanged, the cell was considered to be leak proof. Sometimes, as an additional check, the helium was left in the cell for about a day and the pressure on both the inside and the outside of the cell checked periodically. If the pressure held, the cell was deemed leak-free. The procedure also provided a check on the diffusion of gas through the Mylar. The whole apparatus was then repressurized to atmospheric pressure.

During some of the earlier work, the cell was gradually cooled down to $77^{\circ}K$ by suspending it in the cold nitrogen

vapors contained in a dewar partially filled with liquid nitrogen. The cell was then gently warmed up, reloaded in the vacuum chamber and retested for leaks. The practice was later discontinued because the cells never seem to develop leaks due to cooling.

Next, the leak tested cell was loaded up in the probe as shown in Figure 4 and the probe in turn supported inside the cryostat dewar, in such a way that the cell was well centered between the poles of the magnet as shown in Figure 3. An electrical continuity check was then made on the thermistor and heater leads. The leads were also checked for isolation from ground and from other circuits. After the 0-ring seals were secured, the system was evacuated very slowly by means of a roughing pump till the pressure--as indicated by the Wallace and Tiernan gauge--reached 10 torr. The valves were then fully opened, and when the pressure reached 50 microns--as indicated by the Stokes gauge--the diffusion pump was connected to the system. The probe and the cell were allowed to be evacuated in this manner for a couple of days, during which, the cold trap was kept continuously filled with liquid nitrogen to freeze out the diffusion pump oil vapours and hence prevent them from back diffusing to the cell.

When a pressure of 5×10^{-5} torr. was reached, the probe was cooled down by filling the dewar with liquid nitrogen. The cooling rate was increased several-fold by filling the

probe with helium gas to a pressure of 2 to 4 torr. while keeping the rest of the vacuum spaces, viz. the cell and the dewar, isolated. On reaching a temperature of about $77^{o}K$, as indicated by T1, the helium was pumped out and the high vacuum system was reconnected to the probe, cell and dewar. The dewar was filled to the top with liquid nitrogen, and the whole system allowed to stabilize for 2 to 8 hours as required. During this period, the temperature of the IC was continuously displayed on the strip chart recorder. When a steady drift rate was achieved, the data were taken.

PROCEDURE FOR OBTAINING THE HEAT LEAK CORRECTION FACTOR "L_G", THE THERMAL CONDUCTIVITY OF NITROGEN AND THE ACCOMODATION COEFFICIENT

The following steps comprised the procedure used:

1. The two thermistors T1 and T2 were connected to the opposite arms of the bridge. The multiplication factor dial was turned to the "X1" position, so as to produce about the same heat dissipation in each thermistor. The sensitivity of the null detector and the chart speed of the recorder were set at the appropriate values depending upon the drift rate.

2. The unbalance voltage (and hence indirectly the temperature of the IC relative to that of the OC) was recorded for about 20 minutes so as to obtain the overall drift rate of the probe temperature.

3. The bridge was then balanced, and the resistance read off rom the rheostat arm decade boxes.

4. The inner cylinder heater circuit was then switched on. The power input to the heater was adjusted by adjusting the value of the variable resistance R_V and the supply voltage to give temperature gradient, ΔT, of about $1^{o}K$ between the IC and the OC.

5. When the imbalance voltage resumed its original rate of drift, another null reading was taken.

6. The cell was then filled with nitrogen to a pressure of 10 torr.

7. When the thermal transients due to filling had died out, a null reading was taken (as in step 3), keeping the heat input the same as in step 4.

8. Potential drop reading were across the ICH and the standard 10Ω resistor in order to obtain the heat input.

9. The IC heater circuit was switched off.

10. When the drift rate became steady again, a null reading was taken again.

The difference between the null readings taken in step 3 and step 10, after allowance was made for drift, gave quantitative information on the self-heating due to the thermistor. The difference between the adjusted null readings taken in steps 3 and 5 then was used to calculate the temperature gradient across the evacuated cell and will henceforth be

referred to as ΔT_E. Similarly, the temperature gradient across the cell in the presence of nitrogen (denoted by ΔT_G) is given by the corrected difference between the null readings in steps 7 and 10. These values were then directly used to calculate the heat leak correction factor, L_G, and the thermal conductivity of nitrogen, k_G, as will be shown in Chapger V.

In order to obtain data to help calculate the accomodation coefficient, a_G, the nitrogen in the cell was pumped out in stages, and at each stage a null reading was taken. The data so obtained was used in the calculations involving a_G, For details see Chapter V.

PROCEDURE TO OBTAIN A ΔT SUCH THAT THE MAGNETORESISTANCE OF THE TWO THERMISTORS WAS EQUALIZED

This procedure was necessary because, contrary to expectations, the magnetoresistance of the two thermistors was not equal when their absolute resistances were equal. The reason for this is not clear at the present time. The procedure involved measuring the difference between the magnetoresistance effects of the two thermistors as a function of the difference between the resistances of the two thermistors T1 and T2, $(R_{T1} - R_{T2})$, where R_{T1} and R_{T2} are the resistances of T1 and T2, respectively. The data obtained was then used to determine a value of $(R_{T1} - R_{T2})$ such that the magnetoresistance effect of the two thermistors would be equal. For obvious reasons, the cell had to be filled with a noble gas during the

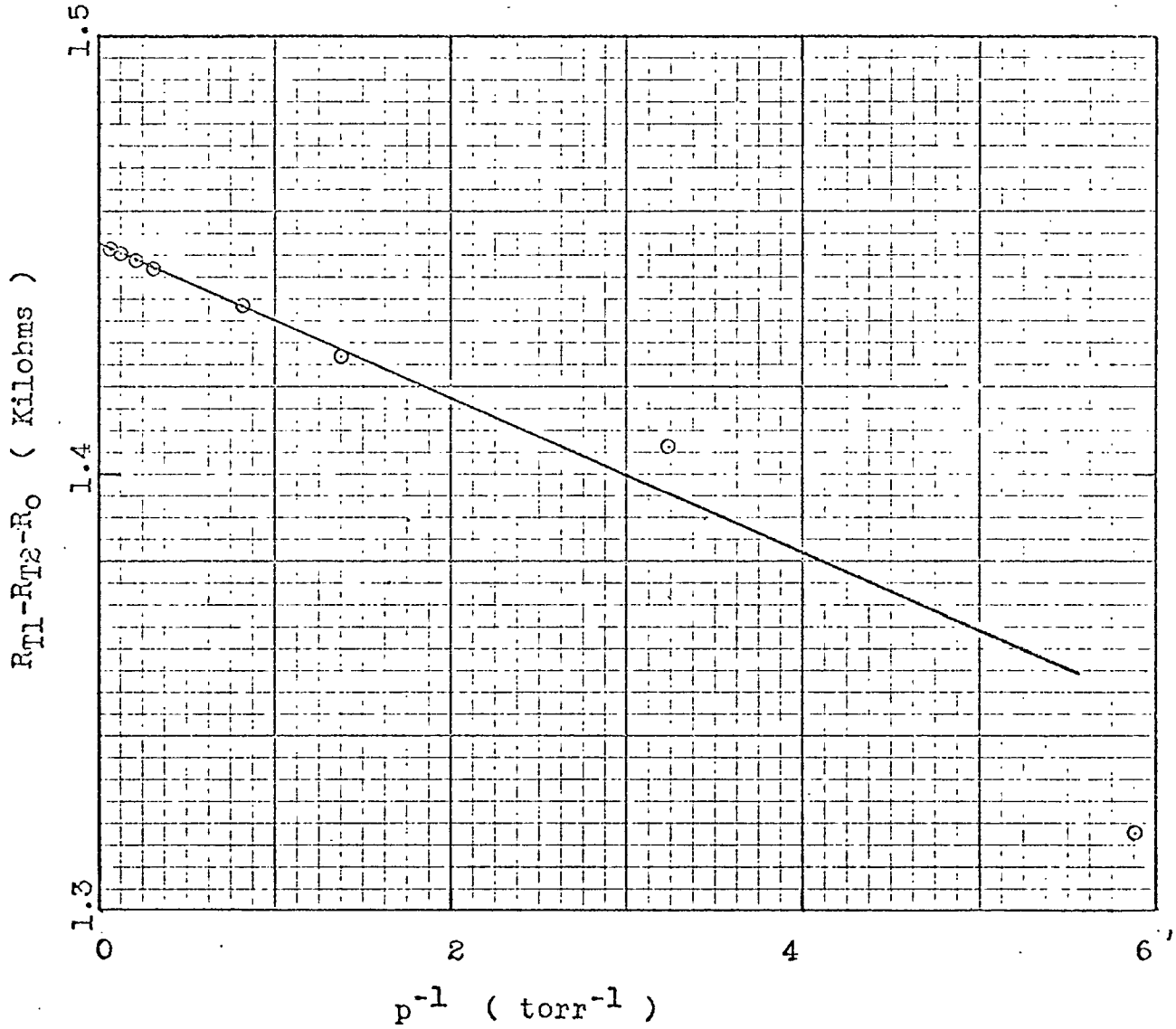

Figure 14: $R_{T1} - R_{T2} - R_o$ Versus 1/p for Nitrogen at a Constant Heat Input to Inner Cylinder

procedure.

The step by step method used was:

1. The cell was evacuated, and then filled with argon to a pressure of 10 torr. Argon was used because it has a conductivity fairly close to that of nitrogen.

2. With T1 and T2 wired into the bridge as before, the ICH circuit switched on, and R_V set to any value, the detector was set to a sensitive scale (like 10 microvolt full scale). The imbalance voltage was monitored by the recorder.

3. The recording was calibrated by introducing a known unbalance and noting the recorder deflection. The bridge and measuring circuits were also checked for linearity.

4. The magnetic field was then turned on to its maximum strength (about 16 Kilogauss) and the steady deflection noted.

5. The field was switched off.

6. The difference in the magneto-resistance effect of the two thermistors, $\delta R_{m(T1 - T2)}$ was calculated from the deflection obtained in step 4.

7. The above steps were repeated with different values of R_V. The data so obtained were plotted as shown in Figure 15. The intercept on the $-(R_{T1} - R_{T2})_o$ for which $\delta R_{m(T1 - T2)}$ is zero.

8. R_V was adjusted to give the value of $-(R_{T1} - R_{T2})_o$ found in step 7, and steps 4-6 were repeated, and indeed $\delta R_{m(T1 - T2)}$ was found to be essentially zero.

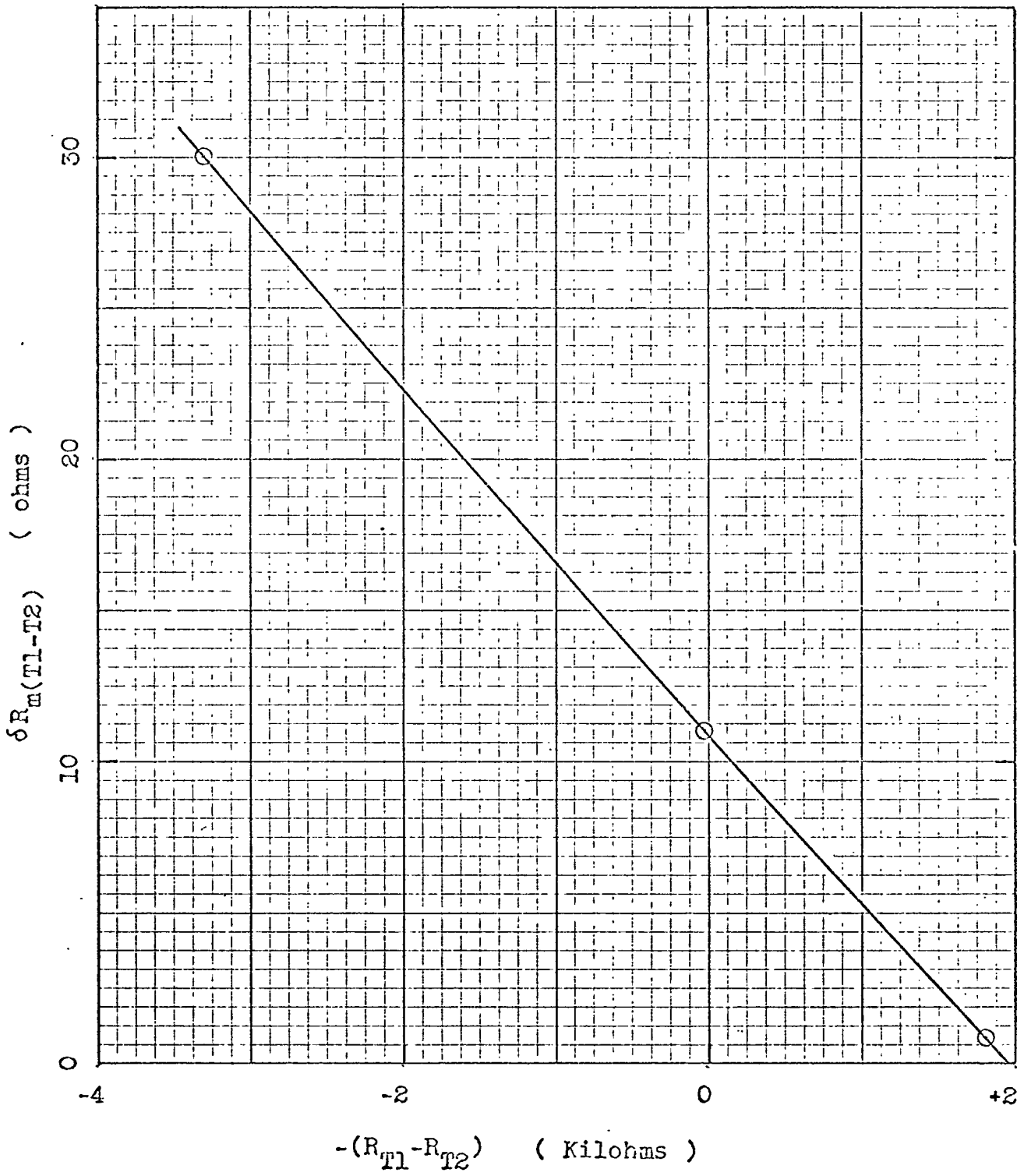

Figure 15: Difference Between the Magnetoresistances of T1 and T2 Versus Their Resistance Difference

Naturally, such a procedure represents a limitation in the sense that, for a given pair of thermistors, a given geometrical configuration and a given operating temperature, the ΔT is fixed; and may in general be too large or too small to use. In fact, if care was not taken in the selection and the positioning of the thermistors, ΔT could even turn out to be negative. Fortunately, during this experiment, for the thermistors used at a temperature of 77.4°K, a value of 5185 Ω was obtained for $(R_{T1} - R_{T2})_o$ corresponding to ΔT of 1.46°K. Operation at this ΔT assumed equality of the magnetoresistance effects for T_1 and T_2. However, the author has devised a method for overcoming these limitations (see Chapter VI).

PROCEDURE FOR OBTAINING SENFTLEBEN-BEENAKKER DATA

1. The cell was evacuated, flushed a couple of times with nitrogen, and then filled with nitrogen to a pressure of about 10 torr.

2. The heat input was adjusted to give a 5185 ± 2Ω difference between R_{T1} and R_{T2}.

3. The imbalance voltage was monitored by the recorder; and when a steady slope was established, the field was switched on, and the output of the magnet power supply adjusted to generate the maximum field.

4. About 5 minutes were allowed to elapse, within which time the recording resumed its original slope. The field was switched off.

5. About 5 more minutes were allowed for the imbalance voltage to resume its original path.

6. The above steps were repeated for successively smaller fields, until the effect became too small to be measured.

7. The recording was calibrated by introducing a known imbalance in the bridge and noting the deflection.

8. The pressure of the nitrogen in the cell was then reduced in stages. At each stage, field effect measurements were made. In this work, the lowest pressure used was 0.25 torr. Lower pressures were not used because the thermal transport seemed to be entering the temperature jump regime. Also, the author mistakenly thought that saturation had been reached.

A reproduction of a typical recorder page is presented in Figure 16. Notice the large spikes when the field is switched on or off. These are due to electromagnetic induction.

Before and after each individual pressure run, readings were taken on the voltage drops across the standard 10Ω resistor and the ICH. These readings were used to calculate the heat input to the cell, and were found to remain constant to within 1 part in 10^4 over a period of 50 hours.

SPECIAL NOTES

During individual runs, care was taken not to do anything that could affect the temperature drift rate. This included filling the dewar, the cold trap on the high vacuum system, stirring the liquid nitrogen bath, moving the leads, blowing

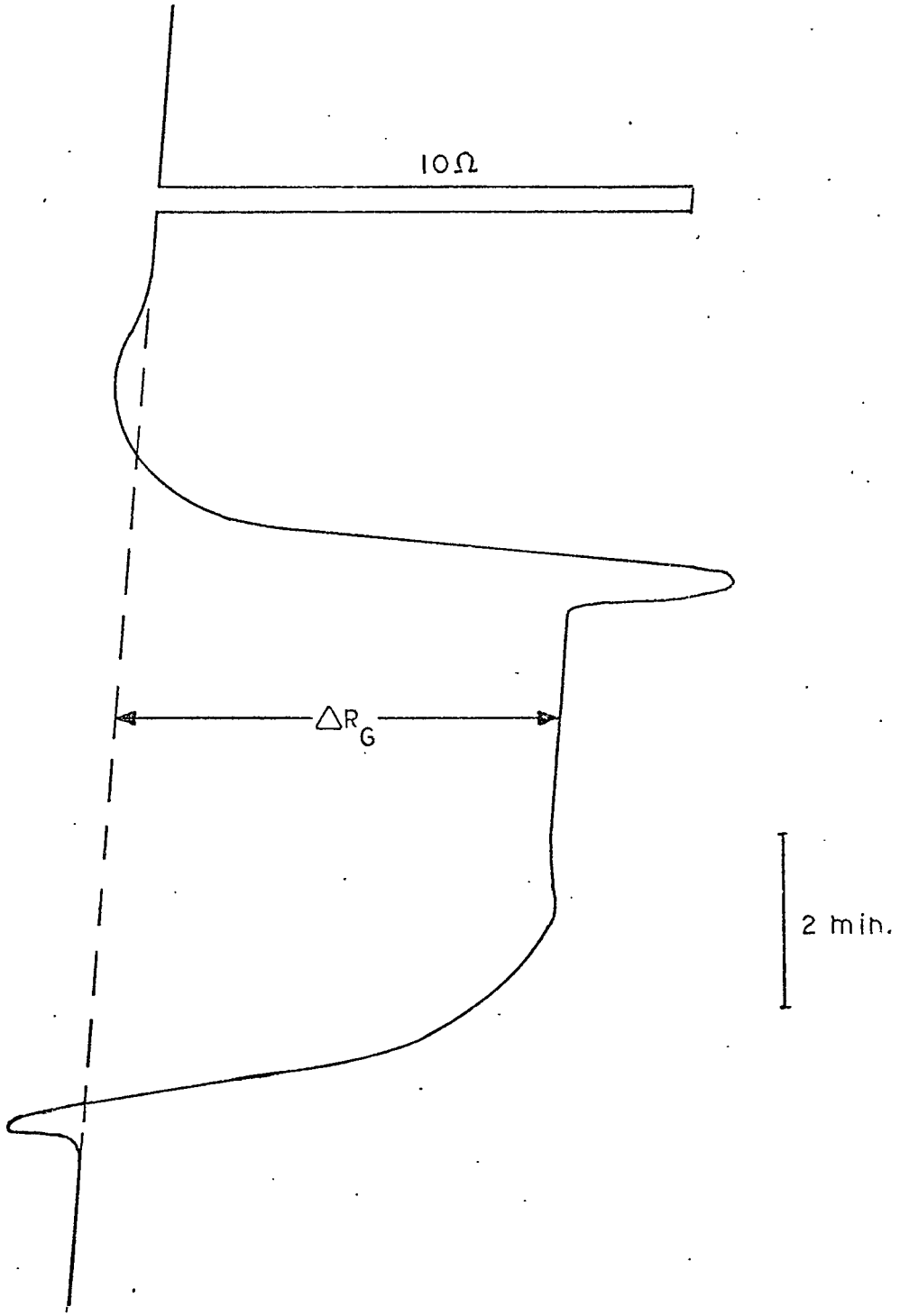

Figure 16: Typical Recorder Output

either warm air or cold vapours over the thermistor leads, etc.

Before the measurements were made, extensive tests were conducted to make certain that none of the measuring instruments were affected by the strong magnetic fields.

CHAPTER IV

THE EFFECT OF MAGNETIC FIELDS ON THE ELECTRICAL RESISTANCE OF TEMPERATURE SENSORS

PURPOSE OF THE STUDY

In making Senftleben-Beenakker effect measurements, it is obvious that the temperature sensors and their leads would be subjected to strong magnetic fields. An exploratory investigation indicated the presence of rather large perturbations caused by magnetic fields on the resistances of low temperature thermistors[36]. These effects have not been previously reported in literature, hence it was decided to conduct a thorough investigation of the effect of magnetic fields on various temperature sensors. The objective was to determine the feasibility of using them in the thermal conductivity apparatus and, if possible, to obtain a mathematical expression relating the effect to the field. It is clear that the magnetoresistance behaviour of the copper leads is of importance, and it too was studied.

DESCRIPTION OF THE APPARATUS

Most of the data presented in this work was taken using the very simple set up shown in Figure 17.

The probe (see Figure 18) consisted of a stainless steel cylinder (C) 2 inches long and 3/4 inch in diameter with a 1/4 inch hole drilled into it. A piece of thin walled stainless

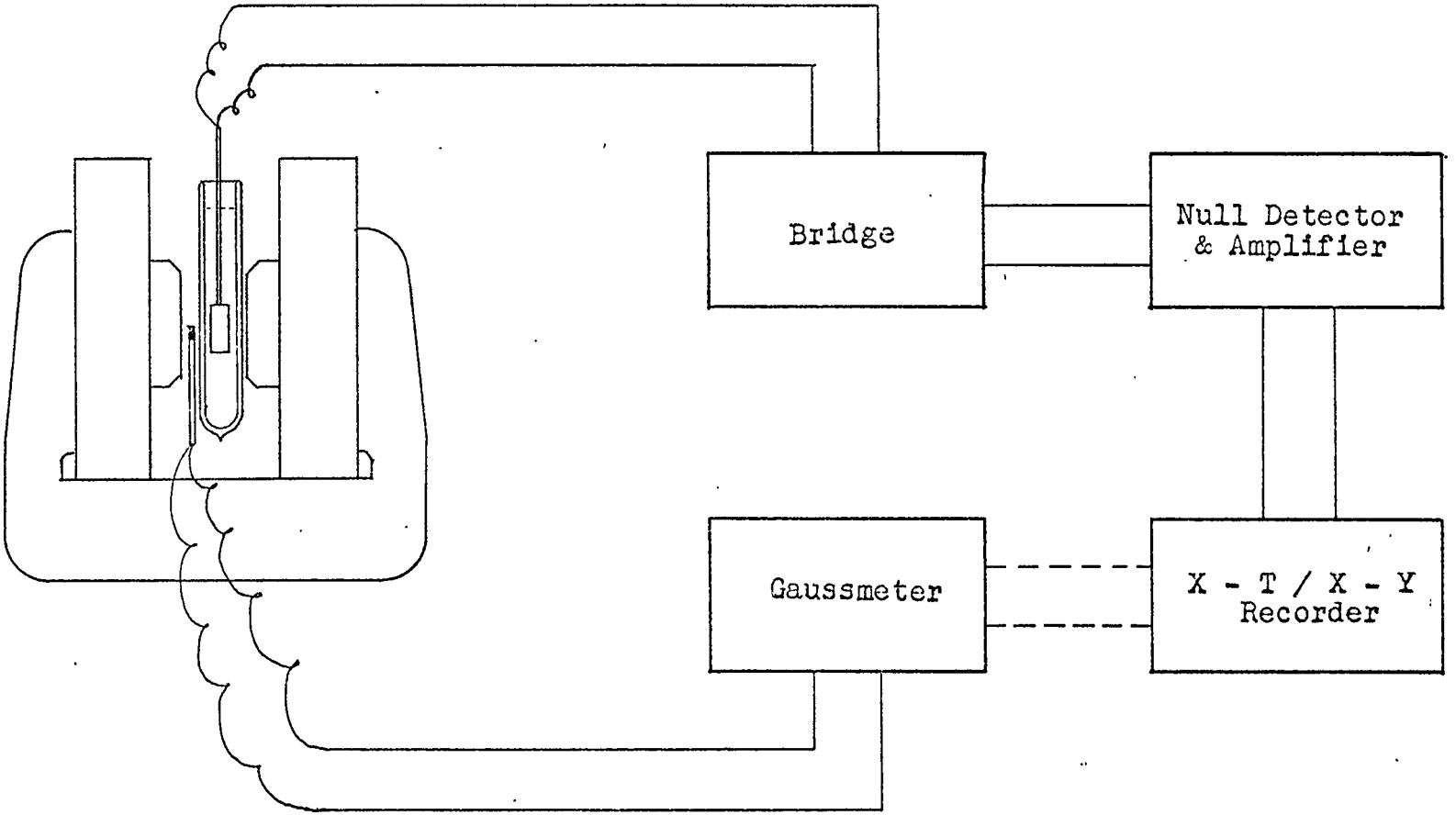

Figure 17: Schematic of the Apparatus

for Obtaining Magnetoresistance Data

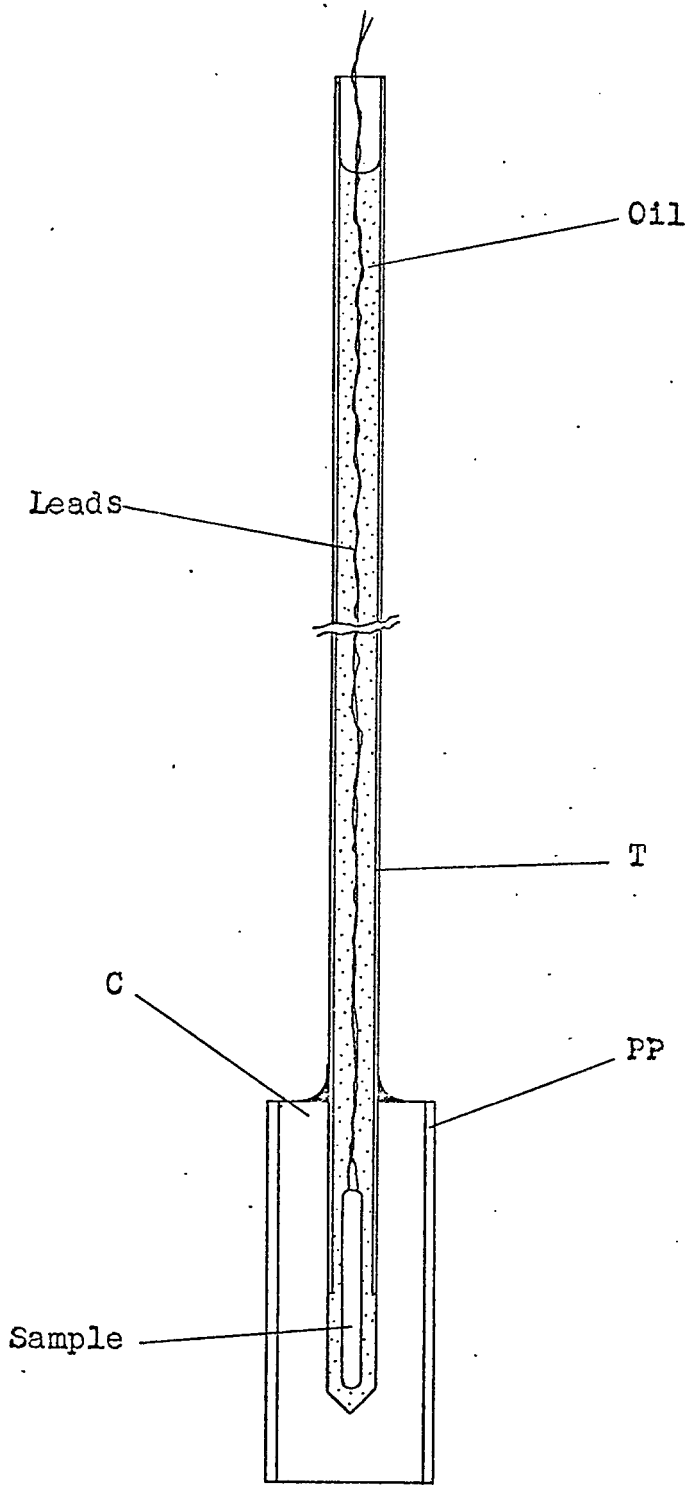

Figure 18: Longitudinal Section Through the Probe
(Overall Length: 16 inches)

tube (T), 1/4 inch in diameter and about 15 inches long was inserted in the hole and soldered in place. Porous paper (PP) was wrapped around the cylinder and the tube. The sensor under study with twisted 18 AWG copper leads soldered to it was inserted into the probe so as to be located approximately in the center of the cylinder. The tube was then filled to the top with diffusion pump oil.

The large thermal mass of the cylinder gave good temperature stability, while the paper helped reduce the effect of surface temperature fluctuations caused by formation of bubbles, local convective currents, etc. The thin walled stainless steel tube reduced heat conduction to the cylinder, and hence helped it to attain the bath temperature as closely as possible. The oil helped maintain good thermal contact between the cylinder and the sensor. At low temperatures, it froze, and hence held the sensor firmly in place. It also kept air and moisture away from the sensor (at a temperature of 77^{o}K, air can otherwise liquify around the sensor and cause severe stability problems).

The probe was placed in a dewar containing an appropriate coolant such as water or liquid nitrogen. The dewar in its turn was supported between the pole caps of the Magnion L-96 Electromagnet.

PROCEDURE

The resistance of the test sample (a temperature sensor

or a coil of wire) was measured in a simple Wheatstone bridge. The unbalance voltage of the bridge was either fed directly to the recorder, or was amplified before doing so as the situation demanded.

The bridge was switched on and the unbalance voltage reflecting the resistance of the sample was continuously recorded. When the resistance reached a steady value, or a steady rate of change of resistance (as indicated by a straight line on the recorder chart), the magnetic field was switched on and the current through the magnet coils adjusted to give the maximum field (about 16 Kilogauss). After the transients had died out and the original rate of drift had been reestablished, the field was switched off. Time was again allowed for the transients to decay and the original rate of drift to be reestablished. The same procedure was repeated for successively smaller fields. The recorder and/or amplifer sensitivities were adjusted whenever needed to yield the maximum accuarcy of measurement.

The steady state deflections so obtained were calibrated from the deflection produced by introducing a known imbalance voltage in the bridge. The absolute resistance was checked by nulling the bridge at regular intervals. The bridge was also checked for linearity and was always found to be linear for the sensitivities used on the instruments. The field was measured by using a Hall effect type Bell (Model 620) gaussmeter.

A much more direct method was however used toward the end of the work. The output of the gaussmeter, the probe of which was placed between the pole caps of the magnet, was used to move the Y-axis of the recorder so that a δR_m versus H plot was directly obtained, where δR_m is the change in the resistance of the sample in the presence of the field H.

For each sensor, an effort was made to study any orientation effects by rotating the probe and looking for a change in the δR_m at a fixed value of the magnetic field.

LIST OF SAMPLES TESTED

1. Low temperature thermistors supplied by Keystone Carbon Co. (Type RL 10X04-10K-315-S5). These were divided into two groups for the purposes of data treatment.

   Group I: Received: August, 1967 (2 numbers)

   Group II: Received: January, 1969 (5 numbers)
2. A copper wire coil made out of 44 AWG magnet wire.
3. Platinum resistance thermometer supplied by Electric Thermometers Inc. (Type G-20).
4. A coil of Evanohm wire

RESULTS AND DISCUSSIONS

1. Figure 19 shows a plot of δR_m versus H for the low temperature thermistors. Some conclusions may be drawn directly from the plots. Firstly, the resistances of the

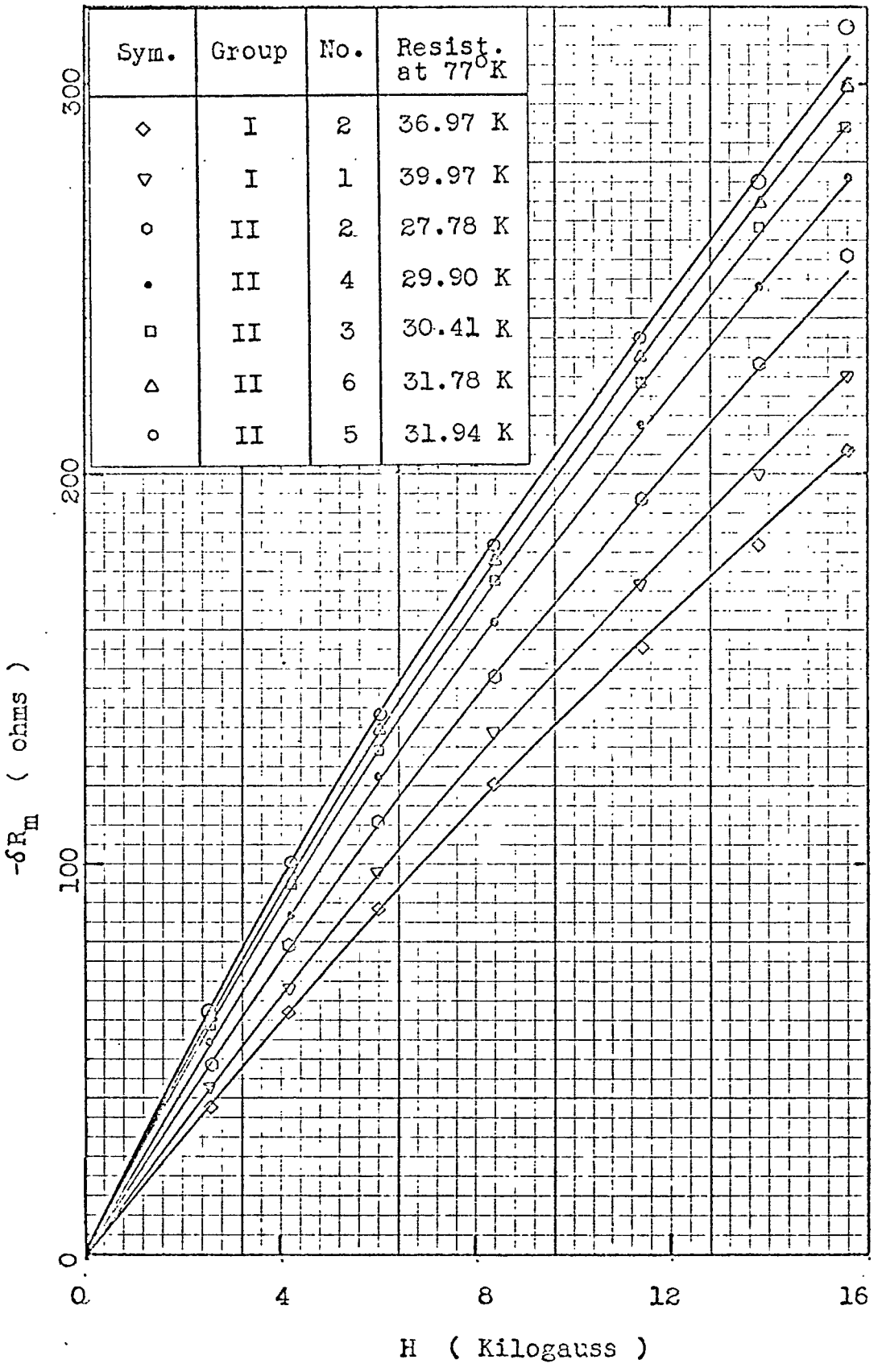

Figure 19: Magnetoresistance of Thermistors at 77.3°K

thermistors decrease as the field increases, and the effect seems to be approaching saturation at high fields. Within each group, it is noticed that the thermistors having higher resistance at the operating temperature display larger magnetoresistance effects. However, though all the thermistors of Group II have a smaller resistance than those of Group I, they display a larger effect. This is difficult to explain. One can only speculate that there is a difference between the chemical compositions of the two batches of thermistors or that possibly there is a connection between the magnitude of the effect and the past history of the thermistors. In this context, it may be mentioned that not only were the Group I thermistors "aged" but that they had been subjected to considerable thermal cycling and to intense fields (up to 100 Gilogauss).

The different curves in each group may be collapsed into just one curve by plotting $\delta R_m/R^{1.25}$ versus H, as shown in Figure 20. No real significance can be attached to this behaviour at the moment. All the data on thermistors were taken at about $77.3^{o}K$.

2. Data on the copper coil were taken at $286^{o}K$ and $77.3^{o}K$. A plot of $\delta R_m/R$ versus H gives two parallel straight lines, B and C, as shown in Figure 21. The two lines, however, merged into just one when $\delta R_m/R$ values were plotted versus S_oH where $S_o = R_{286^{o}K}/R_{T^{o}K}$. This too is demonstrated in the same figure.

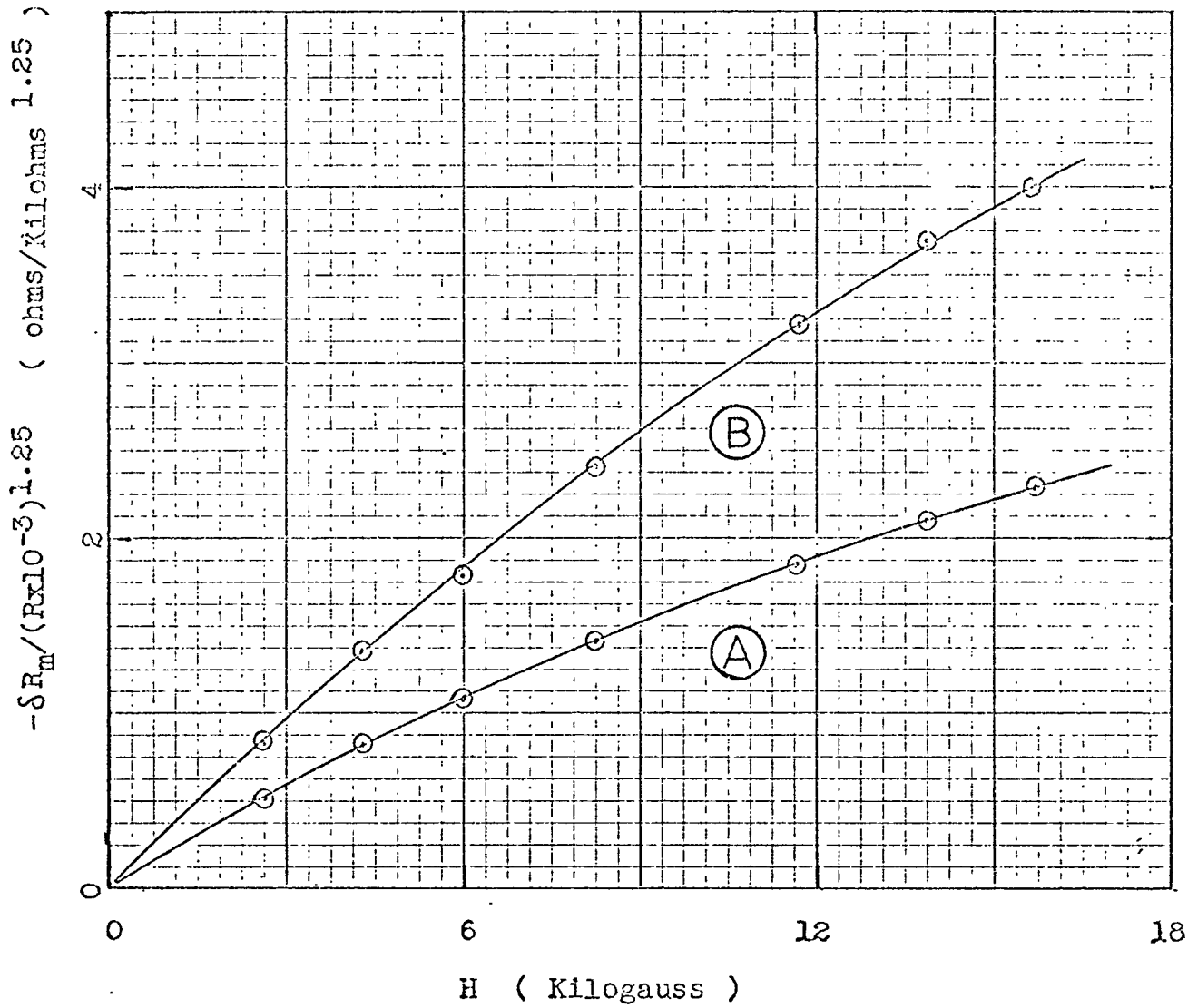

Figure 20: Universal Thermistor Behaviour Versus Field Strength

Curve A: Group I Thermistors Curve B: Group II Thermistors

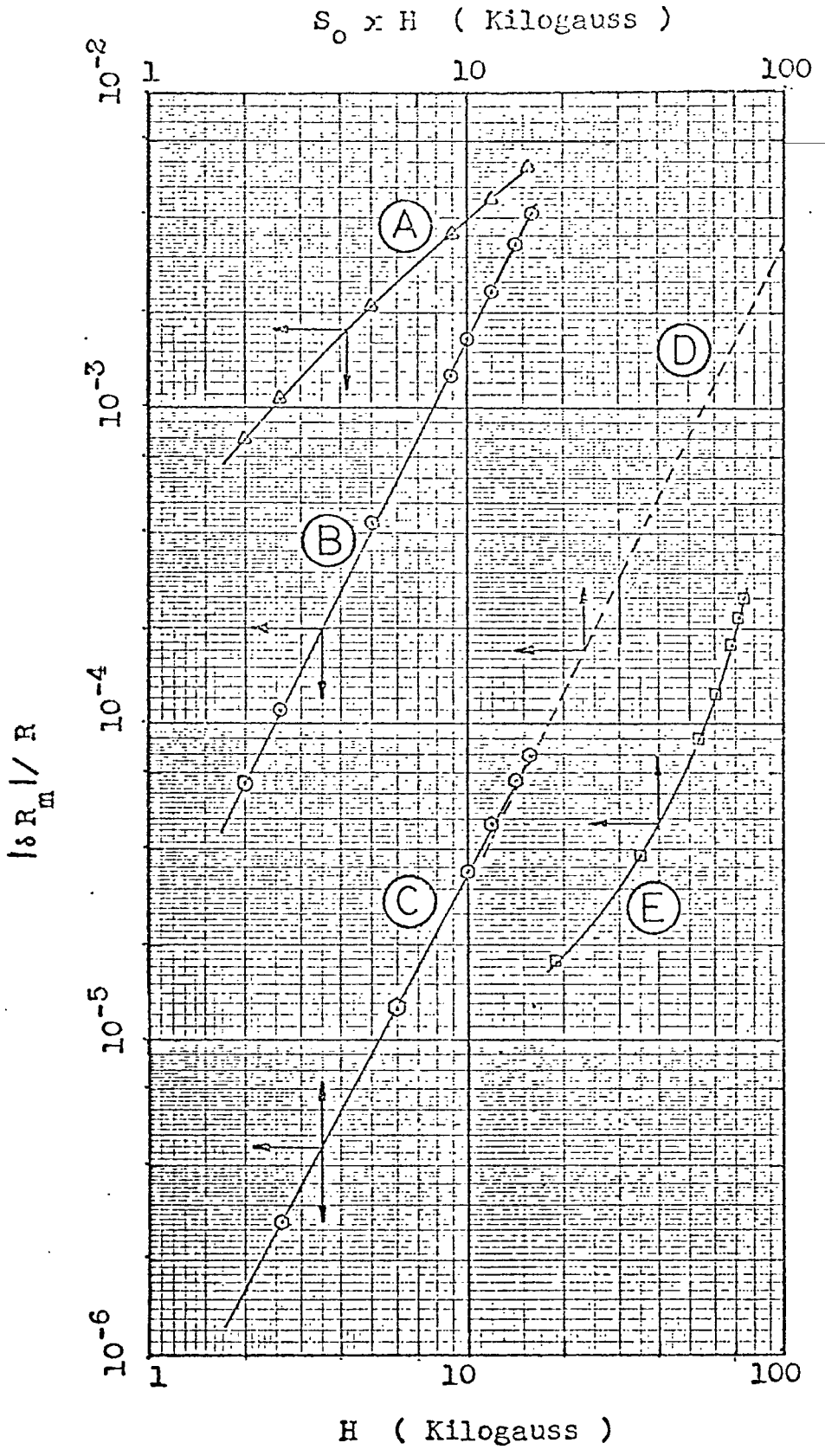

Figure 21: The Magnetoresistance Effect for Various Materials

Curve A: Tl at 77.3°K

Curve B: Cu Coil at 77.3°K

Curve C: Cu Coil at 286°K

Curve D: Cu Coil at 77.3°K

Curve E: PRT at 77.3°K

3. The platinum resistance thermometer showed the smallest effect at 77.3^{o}K as seen from Figure 21. The effect was infact too small to be measured at room temperatures.

4. No measurable effect was found for the coil of Evanohm wire even at low temperatures and high fields.

For the sake of comparison, the magnetoresistance effect data obtained from the thermistor mounted on the inner cylinder of the cell (used in Senftleben-Beenakker effect measurements) is plotted in Figure 21. No orientation effects were found for any of the samples within the limits of experimental accuracy. None of the effects were found to be current dependent within the range of currents used (10-200 microamperes).

CONCLUSIONS

It appears that all electrical conductors display a magnetoresistance effect. The effect seems to be related to the dependence of the resistance of the sample on its temperature. Hence, thermistors, which display the highest sensitivity to temperature, also display the largest effect; while an Evanohm coil, whose resistance is hardly affected by temperature, shows the smallest effect. Platinum and copper take their places in between these two extremes.

The magnetoresistance effect is always such that the sample shows a virtual rise in temperature. Hence, for (negative temperature coefficient) thermistors the effect is negative, while for the platinum thermometer and the copper coil

the effect is positive.

The results of this study indicate that the magneto-resistance effects on the thermistors are large enough to be overwhelmingly dominant in the S-B measurements if they are not compensated for.

Table I compares the change in resistance of the various samples studied due to a field of 16 kilogauss with that produced by a $0.1^{\circ}K$ change in temperature at $77.3^{\circ}K$. The ratio of the two changes in resistance, R_F, provides an index to determine the feasibility of using the sample as a temperature sensor in S-B measurements. Obviously the smaller the value of R_F for a given sample, the better suited it is for use in making S-B measurements.

TABLE I

A COMPARISON OF THE FEASIBILITY OF VARIOUS TEMPERATURE SENSORS IN SENFTLEBEN-BEENAKKER MEASUREMENTS

Sample	$\delta R_m \mid H = 16$ Kilogauss $= X'$ (ohms)	$\Delta R \mid \Delta T = 0.1^{\circ}K = Y'$ (ohms)	$R_F = \frac{X'}{Y'}$
Thermistor No: I(1)	230	400	0.57
Platinum Resistance Thermometer	5.5×10^{-3}	4×10^{-2}	0.14
Copper Coil	1.2×10^{-1}	8.5×10^{-2}	1.4

CHAPTER V

CALCULATIONS, RESULTS AND CONCLUSIONS

CALCULATIONS AND DISCUSSION OF ERRORS

In this section, we shall discuss how the raw data obtained by the procedures described in Chapter III were used in obtaining the final results. The various assumptions involved in making the calculations will be stated, and wherever possible, quantitatively justified. A rudimentary error analysis will be attempted.

The Senftleben-Beenakker effect may be expressed in terms of experimentally measurable quantities by the equation:

$$\frac{\delta k_G}{k_G} = - \left[\frac{\delta T}{\Delta T}\right]_G \left[1 - \frac{(Q/\Delta T)_G}{(Q/\Delta T)_E}\right]^{-1} \qquad [V-1]$$

which is derived in Appendix B. For the sake of brevity, $\left[1 - \frac{(Q/\Delta T)_G}{(Q/\Delta T)_E}\right]^{-1}$ will be denoted by L_G, the heat leak correction factor. For the apparatus used in this work, the symbol δk_G really represents $\frac{1}{2}$ $(\delta k_G^{\perp} + \delta k_G^{\parallel})$, or the mean of the perpendicular and parallel S-B thermal conductivity perturbations at a fixed H/p.

In the derivation of the above equation, it was assumed that convective and radiative heat transfer were negligable. We shall now check the validity of this assumption. Considering the IC to be an entirely convex black body which is totally

enclosed within the probe at 77.3°K, the heat transferred by radiation due to ΔT of 1.5°K was found to be about 5 microwatts compared to the ICH input of about 5.5 milliwatts. Since the cell is filled with nitrogen gas, which is diatomic, the question of reradiation by the gas does not arise[38].

The plot of the resistance of the thermistor on the IC, R_{T1}, versus the inverse of the pressure of the sample gas (nitrogen) is presented in Figure 14. It is seen that the experimental points do not deviate monotonically from the straight line drawn through them even at the highest pressures (up to 15 torr.). Hence, it can be concluded that convection is absent in the range of pressures the cell was operated at [32], as otherwise a sudden rise in R_{T1} would have been observed at the higher pressures.

Next, consider how the heat input to the IC, Q; the temperature gradient across the evacuated cell, ΔT_E; the temperature gradient across the cell with the sample gas, ΔT_G; and the IC temperature perturbation due to the field, δT, are calculated and the possible sources or error.

The thermal energy supplied to the IC comes from two sources. Firstly, the current flowing through the ICH generates about 5.5 milliwatts. Secondly, the small current flowing through T1 causes self heating and dissipates the heat to the IC. If the second contribution was a significant fraction of the total heat input, it could give rise to correspondingly

large errors in the S-B effect measurements. The errors would come from the inability to measure the self heating accurately without upsetting the system. An additional uncertainty would result from the fact that the self heating depends upon the resistance of the thermistor itself, which in turn is considerably affected by the magnetic field. At R_{T1} = 37,000Ω, the Joule heating is estimated by using the bridge equation to be about 50 microwatts, or about 1% of the total heat input. This self heating and its change due to the field is accounted for by repeating the experiment with an inert monatomic gas.

Next, the effect of magnetic fields on the resistivity of the Evanohm ICH is so small that the heat input is not expected to change by more than 0.05% even at the highest field strengths. Finally, the change in thermal conductivity of the leads due to the magnetic field causes a change in the rate of heat leak. However, this is completely accounted for by repeating the experiment with Argon. In conclusion, the heat input to the IC is known to within 0.5% for the conditions of the experiment.

The temperature gradients between the IC and the OC with and without the gas, viz. ΔT_G and ΔT_E, are calculated by multiplying the corresponding ΔR_G and ΔR_E by an average dT/dR_T which is obtained from the thermistor calibration curve (see Figures 10 and 11). The decade boxes wired into the bridge have a tolerance of 1% and the average slope could be off by

0.5%[35]. The largest source of error, however, comes from the uncertainty associated with the temperature drift of the probe. The drift rate is obviously a function of the heat input, Q, and several other variables, many of which are beyond experimental control For example, the barometric pressure fluctuations, dewar vacuum fluctuations, the oxygen content of the liquid nitrogen in the bath, and the change in the flow patterns of bubbles of nitrogen vapour as they ascend in the cryostat due to the magnetic field--all these affect the rate of the temperature drift. The uncertainity of the drift rate affects ΔT_E more than it does ΔT_G because with the cell evacuated, the IC has a long time constant. Errors as large as ±100Ω or 2% could occur in ΔR_E. A method has since been devised by the author to overcome this difficulty. (See Chapter VI.) For this work, a maximum overall error of 5% is estimated for L_G and an error of 2% at most in ΔT_G.

The perturbations in temperature of the IC, δT_G, due to the magnetic field effect on the gas, are calculated by multiplying the number of divisions of the deflection obtained on the recorder by a resistance calibration factor, and then by dT/dR_{T1}. The only errors that could therefore be associated with δT_G are human errors in estimating the deflection error in the resistance calibration, and error in the slope. The first type of error is assumed to be random and hence not of much concern. This type of error is reflected in the scatter

in the data points. The second of course gives rise to systematic errors, but it may be reduced by cross checks on the resistance bridge and recorder calibration. Finally, the slope of the thermistor calibration curve also gives rise to systematic errors, but since the temperature perturbations are very small and the thermistors are calibrated over a very wide temperature range, error due to incorrect slope will be small indeed. On the whole, an error of 1% of $(\delta T_G)_S$ may be associated with δT_G.

The calculated quantities Q, ΔT_G, ΔT_E, and δT_G are substituted into equation [V-1] , and $\delta k_G/k_G$ is calculated for each experimental value of the parameter H/p. The results so obtained are plotted on the semi-log graph shown in Figure 22. The magnetic field strength, H, is measured directly by the gaussmeter to within 1%, and the sample pressure, p, is measured to within 2% by the pressure gauges. Random scatter is however possible due to limitations in reading the dials of the instruments. The curve drawn through the data points is the theoretical curve obtained from the Kagan vector contributions. The equation to the curve is of the type[25]:

$$Y = A\left[3\,\frac{B^2X^2}{1 + B^2X^2} + 2\,\frac{4B^2X^2}{1 + 4B^2X^2}\right] \qquad [V\text{-}2]$$

where A and B are adjustable parameters.

The curve yields two theoretically important quantities: the saturation value of the S-B effect, $(\delta k_G/k_G)_S$, and the H/p

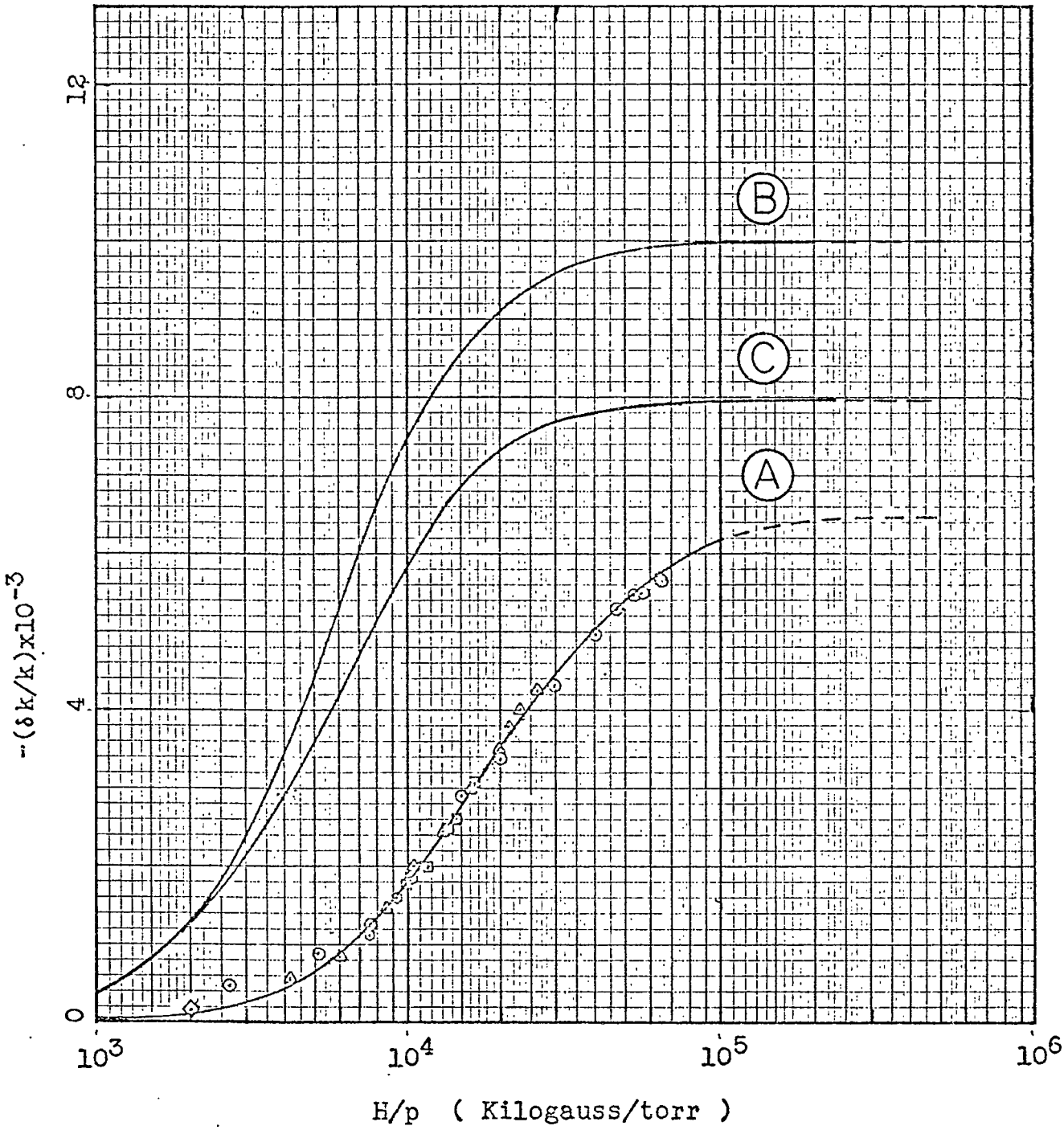

Figure 22: Senftleben-Beenakker Effect for Nitrogen

Curve A: Theoretical Curve Through Data at 78°K

Curve B: Result Obtained by Hermans, et al.[41] at 300°K

Curve C: Result Obtained by Korning[32] at 300°K

value at half-saturation, $(H/p)_{\frac{1}{2}}$. The magnitude of the saturation values is affected by systematic errors in Q, ΔT_E, ΔT_G and δT_G, while the magnitude of $(H/p)_{\frac{1}{2}}$ is affected by the accuracy of measurement of H and p. Generally, it is difficult to obtain $(H/p)_{\frac{1}{2}}$ with an error smaller than 5% because the data is spread over almost two decades, which makes the position of $(H/p)_{\frac{1}{2}}$ difficult to locate. Of course, in the case of oxygen or nitric oxide, the saturation value of the effect is well known, hence determination of $(H/p)_{\frac{1}{2}}$ is possible with greater confidence.

Considering the above, it is reasonable to say that the magnitude of $(\delta k_G/k_G)_S$ was obtained in this work to within 10%; and $(H/p)_{\frac{1}{2}}$ obtained to within 5%. However, improvement in equipment and data handling techniques as ennumerated in the next chapter is certain to give a smaller expected error.

Before going on to the presentation of results, it is important to investigate another potential source of error related to the pressure of the sample gas. To understand the nature of this error, it is useful to distinguish four different gas pressure regimes depending upon the value of the ratio of the mean free path of the molecules, l, and a characteristic heat transfer dimension of the cell, d. The ratio is, of course, the well known Knudsen number, Kn. In the case a cell of parallel infinitely wide plates, the different heat conduction regimes are characterized by the Knudsen number

alone. But for concentric cylinder types of cells, a further complication arises in that the regime is determined not only by Kn, but also by the ratio of the radius of the OC to the radius of the IC, denoted by r*, and the accomodation coefficient of the IC, a_i, given by:

$$a_i = \frac{E_i - E_r}{E_i - E_w} \qquad [V-3]$$

where, E_i = the translational energy possessed by a gas molecule before striking the IC

E_r = the translational energy possessed by the gas molecule after striking the IC

E_w = the translational energy the molecule should have carried if it had completely adjusted or "accomodated" its energy to the temperature of the IC.

Since the translational energy of a molecule is proportional to its absolute temperature, a_i may be rewritten as:

$$a_i = \frac{T_i - T_r}{T_i - T_w} \qquad [V-4]$$

Experimentally, accomodation coefficients have been reported to be a function of several parameters[39], some of which are difficult to characterize quantitatively. They have been found to depend upon the nature of the gas molecules, the molecular structure of the solid wall on which the accomodation occurs, the geometrical shape of the solid, its cleanliness, etc.

The extent of the various regimes is beautifully summarized by Springer and Rytoni[44] in a diagram reproduced in Figure 23, for translational accomodation only.

When the pressure of the sample gas in the cell is reduced, its mean free path increases for a fixed temperature. In fact, for nitrogen, at 77.3°K,

$$l = 2.413 \times 10^{-3}/p \text{ cm.}^{(40)} \qquad [V-5]$$

where p is the pressure of nitrogen (in torr.). The equation is plotted in Figure 6 for quick reference. For a given cell, as the pressure is decreased from large values, the thermal behaviour of the gas eventually enters the temperature jump approximation regime. In this approximation, an apparent decrease of the thermal conductivity is observed because the mean free path of the gas molecules, though small, is no longer negligible compared to the annular gap between the cylinders. Hence, a discontinuity is introduced in the temperature profile near the walls as shown qualitatively in Figure 24. The region over which the discontinuity extends is called the "temperature jump distance", and is usually a few mean free paths long.

Consider now how the phenomenon affects the S-B effect measurements. Recall from Chapter I that $\delta k_G/k_G$ is a unique function of $\omega_L\tau$ and hence of H/p. At high pressures, $l << (r_o - r_i)$, the number of gas-wall collisions is relatively small compared to the number of gas-gas collisions and τ may

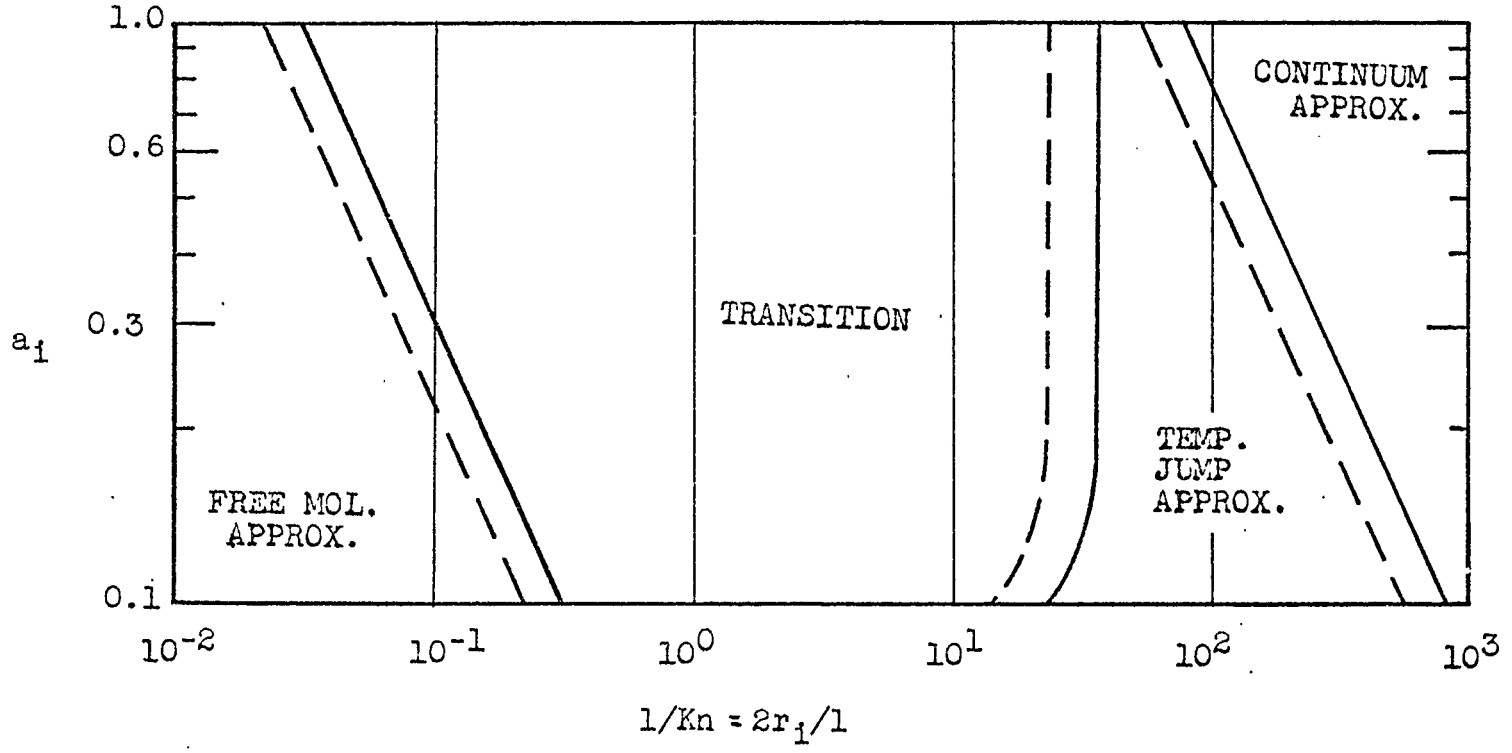

Figure 23: Heat Transfer Regimes for a Dilute Monatomic Gas[44]

——— Boundary for r* = 100

------ Boundary for r* = 1000

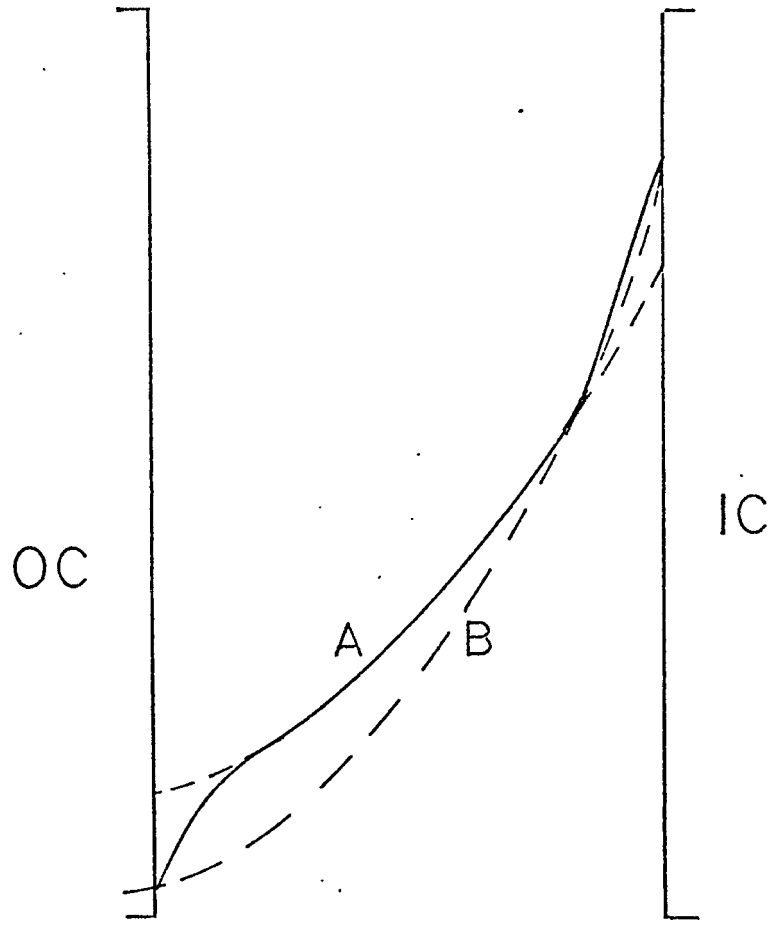

Figure 24. Effect of the Temperature Jump on the Temperature Profile Near the Walls

Curve A: Actual Profile Curve B: Profile if Temperature Jump is Neglected

then be assumed to be inversely proportional to p. However, at lower pressures, the collisions with the wall become more frequent, thus causing the mean free path time, τ, to be no longer inversely proportional to p. Hence the actual value of $\omega_L\tau$ is smaller than that calculated from H/p. The net consequence of which is that $\delta k_G/k_G$ is no longer a unique function of H/p--a fact confirmed experimentally by Hermans, et.al. (41).

In order to determine the possible magnitude of the error caused by the temperature jump, a simple calculation was made.

According to Kennard (34)

$$\left[\frac{\Delta T}{Q}\right]_G = \frac{\ln \frac{r_o}{r_i}}{2\pi L\, k_G} + \frac{g\left[\frac{1}{r_o} + \frac{1}{r_i}\right]}{Lp} \qquad [V-6]$$

$$\text{i.e. } \left[\frac{\Delta T}{Q}\right]_G = \frac{\ln \frac{r_o}{r_i}}{2\pi L\, k_G} + \frac{g'}{p} \qquad [V-7]$$

where, $g = g(a_G)$ and $g' = \frac{g}{L}\left[\frac{1}{r_o} + \frac{1}{r_1}\right]$. g' is obtained from the slope of the line in Figure 14 by multiplying it by the appropriate conversion and calibration factors. Calculations showed that at p = 0.25 torr. about 2.4% of the total resistance to heat transfer offered by the gas comes from the temperature jump region. Hence, the correction to be applied in our case is small. But, for light gasses like hydrogen at higher temperatures and lower pressures, the correction could become quite large.

A final source of error is the change in thermal conductivity of the gas as its log mean temperature changes in presence of the magnetic field. Figure 26 shows the variation of thermal conductivity of nitrogen with temperature. Calculations for our cell, using the slope of the graph in Figure 26 show that the change of the conductivity at saturation is about 0.5% of the S-B effect at saturation. Again, this is a small correction and can easily be applied.

RESULTS AND DISCUSSIONS

The above calculations yield the following numerical results for our experiment:

$Q = 5.54$ milliwatts

$\Delta T_G = 1.46^{\circ}K$

$g = 2.56 \times 10^{-3}$ dyne sec $^{\circ}K/erg\ cm^2$

$Q_{RAD} = 5$ microwatts

$Q_{TH} = 50$ microwatts

$Q_T = 5.6$ milliwatts.

These give the following values for the cell performance criteria:

$L_G = 1.672$

$k_G = 0.82$ microwatts/cm $^{\circ}K$,

where, L_G is the heat leak correction factor, and k_G is the thermal conductivity of nitrogen calculated by using [B8]. From the value of L_G it may be deduced that about 40% of the total heat input to the IC is dissipated by means other

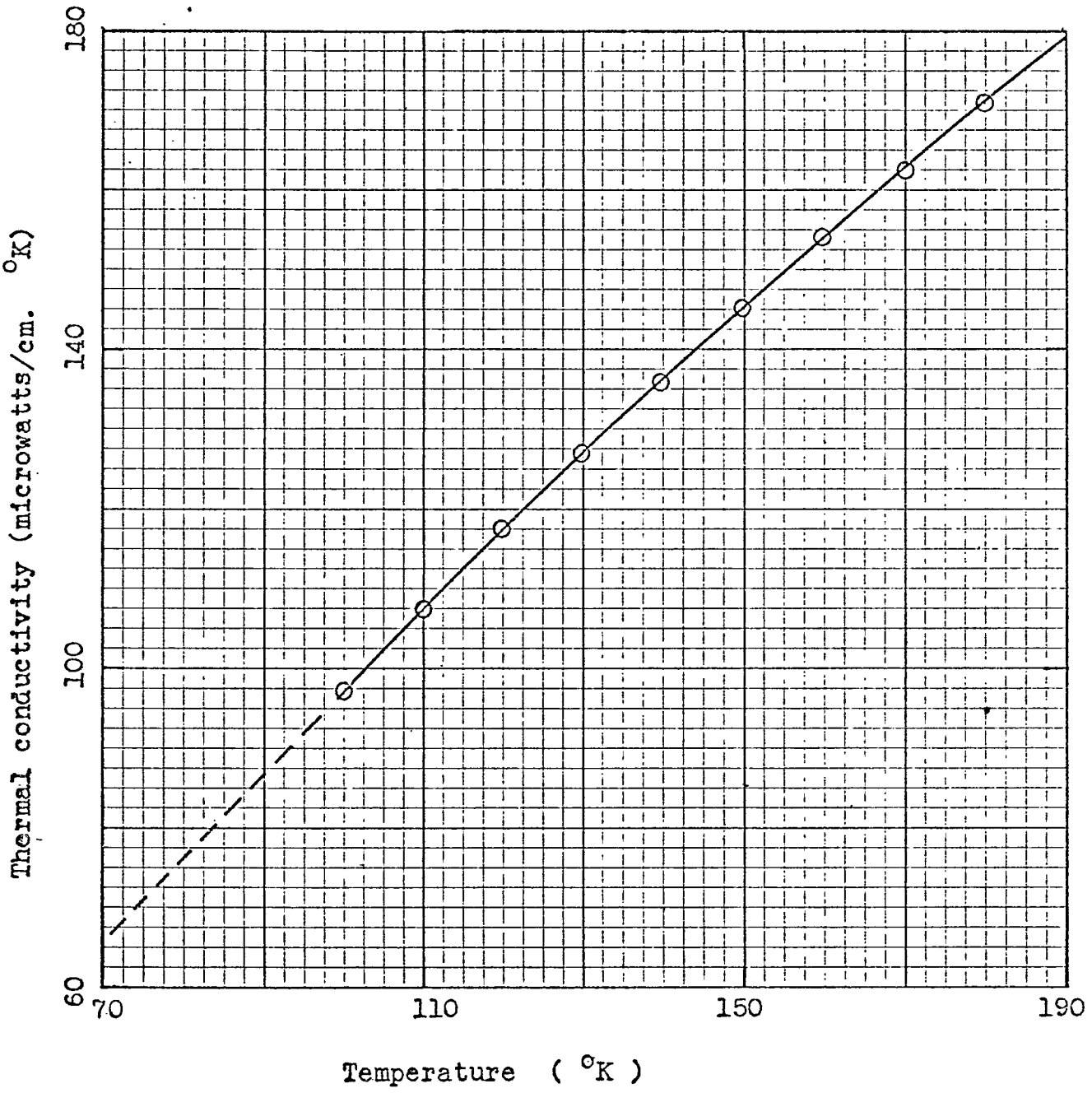

Figure 25: The Variation of the Thermal Conductivity of Nitrogen with Temperature

than conduction through the gas. The value of the thermal conductivity of nitrogen obtained is high compared to the literature value of 0.74 microwatts/cm ^{o}K obtained from Figure 26.

Consider again, Figure 22 which shows the S-B data points for nitrogen. Line A is a theoretical curve based on Kagan vector type polarizations only. It has been passed through the data points by suitably choosing the adjustable parameters A and B of [V-2]. It is seen from the figure that data taken at different pressures do not show significant systematic deviations as might be expected had we ventured into the temperature jump regime. Curve B shows the experimental results obtained by Hermans, et.al.[41] at 300^{o}K. Their results are compared with the present work by taking the mean of the results they obtained for $\delta k_G^{\perp}/k_G$ and $\delta k_G^{\parallel}/k_G$. Curve C shows the result obtained by Korving[32] at 300^{o}K. The cause of the difference between the data obtained by Hermans and Korving is not quite clear. However, it may be noted that while Hermans used a parallel plate cell, Korving used a concentric cylinder type of design with rather complicated end seals.

The data obtained in this work shows a more or less significant reduction in $(\delta k_G/k_G)_S$ and a fairly large increase in $(H/p)_{\frac{1}{2}}$ even after error bands are added to the data. A comparison of the significant differences is given in Table II.

TABLE II

COMPARISON WITH LITERATURE DATA

FOR NITROGEN

Investigator(s)	Temperature (°K)	$(H/p)_{\frac{1}{2}}^{(1+\Pi)/2}$ Kilogauss/torr.	$-\left[\frac{\delta k_G}{k_G}\right]_S^{(1+\Pi)/2} \times 10^3$
Korving[32]	300	5.3	7.9
Hermans, et.al.[41]	300	5.7	10.0
This work	78	18.5	6.5

Now, for the Kagan vector polarization[25],

$$\left[\frac{\delta k_G}{k_G}\right]^{(\perp + \parallel)/2} = \psi \left(3 \frac{\theta^2}{1 + \theta^2} + 2 \frac{4\theta^2}{1 + 4\theta^2} \right) \qquad [V\text{-}8]$$

Using this equation, it may be easily shown that the effect reaches half its saturation value at $\theta = 0.762$. Therefore, from the definition of θ,

$$\left[\frac{H}{p}\right]_{\frac{1}{2}}^{(\perp + \parallel)/2} = 0.762 \frac{h}{|g_L| \mu_N} \left\{ \frac{8\sqrt{\pi} \sigma^2 \Omega^{(1,1)*}}{3\sqrt{mkT}} \right\} \qquad [V\text{-}9]$$

The quantity $\Omega^{(1,1)*}$ is a dimensionless integral and is defined as the ratio of $\Omega^{(1,1)}$ to $\Omega_{HS}^{(1,1)}$. $\Omega^{(1,1)*}$ has been calculated and tabulated for various forms of the intermolecular potential by Hirschfelder, et al.[30] The value of $\Omega^{(1,1)*}$ decreases as the absolute temperature increases, hence $(H/p)_{\frac{1}{2}}$ may be expected to increase as the temperature decreases.

The smaller value of $(\delta k_G/k_G)_S$ obtained in this work as compared to others is more difficult to explain. Firstly, there is disagreement between the literature values at 300°K. Secondly, a slight tendency toward a decrease in the effect with decrease in pressure was observed. This indicates the possibility of Knudsen effects. Thirdly, in this work data points were obtained up to 90% of the "saturation value" necessitating extrapolation to obtain the result.

In principle at least, the magnitude of $(\delta k_G/k_G)_S$ would be expected to decrease as the temperature decreases. This is

so, because the contribution of the internal degrees of freecom to the heat transfer mechanism decreases with temperature. Hence, the inelastic collision cross section may be expected to reduce, resulting in the reduction of the saturation value of the effect. In the case of nitrogen, the characteristic temperature for the rotational mode, θ_{ROT}, is 2.9°K; so even at 78°K, the rotational modes may be expected to be fully developed. This means that the above mentioned expected reduction would be too small to account for the actual decrease in $(\delta k_G/k_G)_S$. Further, $(\delta k_G/k_G)_S$ is difficult to calculate theoretically even for the elastic model because it involves several collision integrals and also such uncertain quantities as the non-sphericity parameter[25].

In conclusion, with the information available it is not possible to give a satisfactory explanation for the observed reduction in $(\delta k_G/k_G)_S$.

Let us now turn our attention back to the value of $(H/p)_{\frac{1}{2}}$. This half-saturation value is important from a theoretical standpoint because it depends upon only one collision integral, $\Omega^{(1,1)}$, which can be easily calculated. Using equation [V-9] a value of 10.6 Kilogauss/torr. was obtained for $(H/p)_{\frac{1}{2}}$ in the case of nitrogen at 78°K. Listed below are the parameters used in making the calculations:

Parameter	Value	Source
g_L	0.28	Chan, et al.[43]

Parameter	Value	Source
σ	3.681 Å	Hirschfelder, et al[30]
ε/k	91.5°K	Hirschfelder, et al[30]

Hence, comparing the experimental and theoretical values,

$$\left[\frac{(H/p)_{\frac{1}{2}}^{exp.}}{(H/p)_{\frac{1}{2}}^{el.th.}}\right]_{78^{\circ}K} = \frac{18.5}{10.6} = 1.74.$$

i.e., $$\frac{\text{Experimental coll. integral}}{\text{Elastic Theory coll. integral (Kagan)}} = 1.74$$

This value is compared with the ones obtained by Korving and Hermans, et al. at different conditions in Table III.

Before any effort is made to interpret the above, it must be clearly understood that the elastic theory calculations for which the above calculations are made include the decay of the Kagan type polarization only. This is not an entirely valid assumption, because higher order contributions of the $[\bar{C}][\bar{J}]$ and the $[\bar{C}]^3\ [\bar{J}]^4$ type, though expected to be small, are present.

The closeness of the value obtained in this work at 78°K and that obtained by Hermans at 300°K implies that the variation of the inelastic collisional integrals with temperature closely resembles that of the elastic collisional integrals with temperature. The high values for the transverse effect indicate greater inelastic contributions occur in that effect.

In Figure 26 the S-B effect results for N_2 are plotted on a probability paper. The ordinate is constructed in such

TABLE III

A COMPARISON OF THE RATIO OF EXPERIMENTAL TO THE ELASTIC THEORY COLLION INTEGRAL OBTAINED BY VARIOUS INVESTIGATORS

Investigator(s)	Temp. (^{o}K)	Ratio	Value
Korving	300	$\left[\frac{(H/p)^{exp.}_{\frac{1}{2}}}{(H/p)^{el.th.}_{\frac{1}{2}}}\right]^{(\perp+\parallel)/2}$	1.59 (32)
Hermans, et al.	300	$[\ \text{"}\ ]^{(\perp+\parallel)/2*}$	1.75 (41)
Hermans, et al.	85	$[\ \text{"}\ ]^{T}$	2.2 (3) 2.04 (2)
This work	78	$[\ \text{"}\ ]^{(\perp+\parallel)/2}$	1.74

*Calculated from the corresponding ratio for the perpendicular effect above.

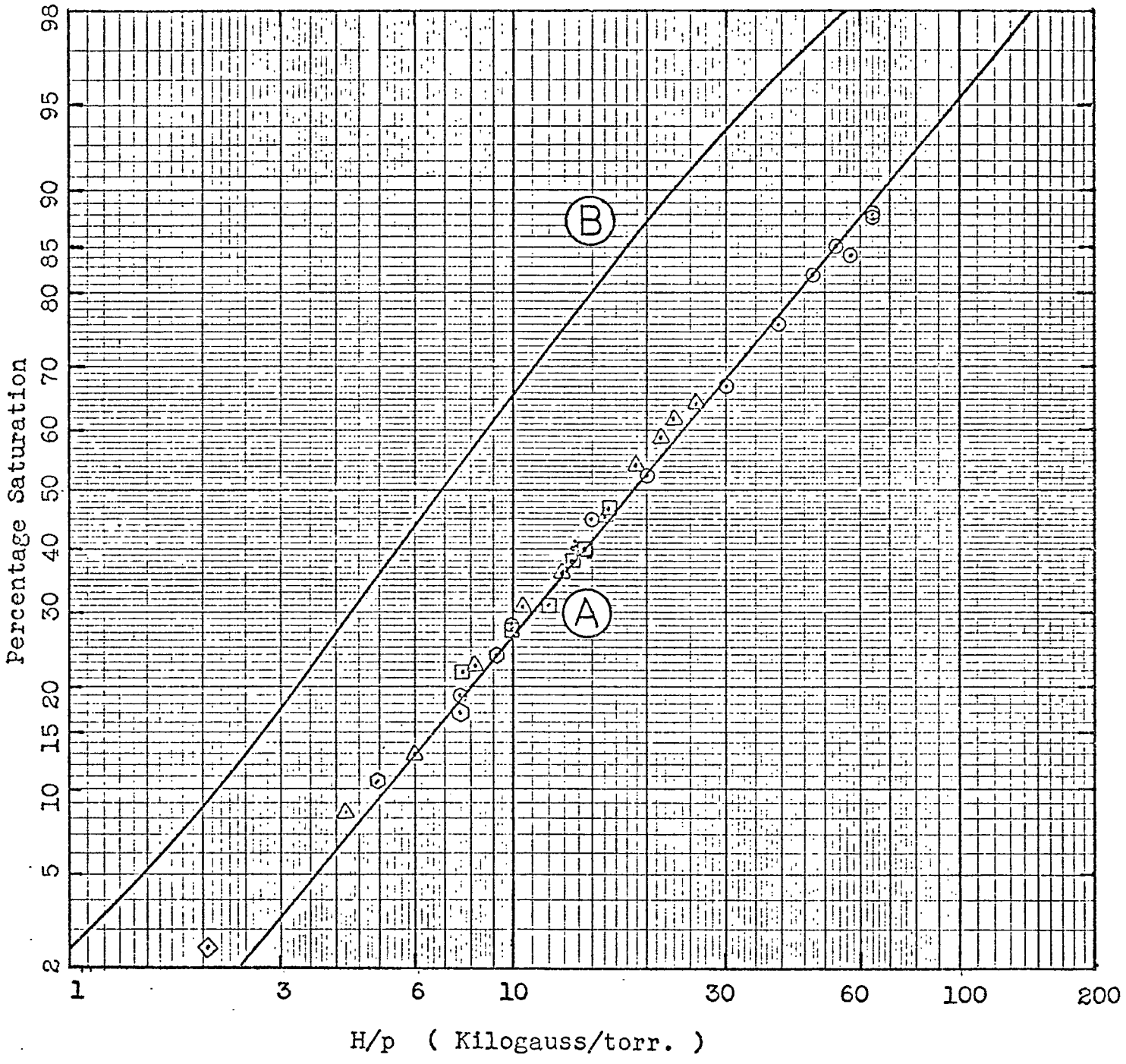

Figure 26: Percent Saturation of Thermal Conductivity Effect as a Function of H/p

Curve A: Straight Line Through Data

Curve B: Theoretical Curve Plotted at an Arbitrary Position on the H/p Axis

a way that the area under a Gaussian curve up to the value x on the abscissa plotted versus the abscissa becomes a straight line. Such a plot effectively linearizes the data. Curve A is a straight line drawn through the data, while curve B is equation [V-8] plotted on an arbitrary position of the abscissa Such a plot allows one to check the projected saturation value and give an accurate value of $(H/p)_{\frac{1}{2}}$.

CONCLUSIONS

The data obtained at low temperature in this work is compatible with that obtained by other researchers at room temperatures. The reduction in the saturation value of the S-B effect is larger than expected. The presence of Knudsen effects may be responsible for the anomaly.

The available theoretical description of the effect has not yet reached a stage where experimental data may be actually used to estimate the values of the collision integrals. Hence, an exact comparison of the various models of the transport process is not yet possible.

CHAPTER VI

RECOMMENDATIONS

Several suggestions may be made both as to the direction of future research and to the improvements in the apparatus and the experimental techniques.

It is recommended that Senftleben-Beenakker thermal conductivity measurements be made on other gases not only at cryogenic temperatures but also at room temperatures. This will provide a direct basis for comparison of work done by this research group with the results obtained by other investigators. Also, it will provide a better basis for studying the variation of the inelastic transport contributions with temperature by eliminating any discrepancy due to differences in apparatus. Also, oxygen is reported as having a very peculiar temperature dependence, while methyl cyanide has been reported to show a positive effect. These gases are interesting to study from a theoretical view point. Methane, ammonia, hydrogen and their deuterated counterparts are also worth studying because fairly good theoretical models are now available for them.

To study the contributions made by the decay of polarizations other than the Kagan vector, a careful study of the ratio $\delta k_G/\delta k_G$ is suggested. Of course, to do this, one either needs a parallel plate cell or the one already constructed used in different orientations with respect to the field. Obviously,

good resolution and small systematic errors will be of prime importance for such measurements.

The present experimental apparatus could be improved to make the above study possible by using platinum wire sensors, which have a smaller magnetoresistance effect. Also, the reference sensor may be arranged in such a way that operation at several different temperature differences is possible, at each one of which, the net magnetoresistance effect may be experimentally adjusted to zero. Further, the end effects of the cell may be accounted for by using cells of different lengths and extrapolating the data so obtained to a cell of infinite length. Finally, the confidence in the saturation value of the effect could be considerably increased if the Knudsen effects are accounted for, and if the heat losses were better known. The heat losses could be accurately accounted for by filling the cell with different gases and using the literature values of their thermal conductivities to extrapolate to zero conductivity. The value so obtained would give a more accurate value of the heat flux per unit temperature gradient across the evacuated cell, $(Q/\Delta T)_E$.

All the above suggestions are quite easy to implement with only minor modifications on the probe.

APPENDIX A

DERIVATION OF THE THERMAL CONDUCTIVITY MATRIX FROM THE PRINCIPLES OF IRREVERSIBLE THERMODYNAMICS AND ITS APPLICATION TO VARIOUS GEOMETRIES

DERIVATION OF THE THERMAL CONDUCTIVITY MATRIX

The entropy production in an irreversible system may be shown to be a sum of bi-linear terms such as $\sum_i J_i \,(\cdot)\, X_i$ where J_i is a generalized flux and X_i is a generalized thermodynamic force. $(\cdot)$ denotes a product appropriate to the tensorial order of J_i and X_i. Furthermore, it may be shown that no fluxes and thermodynamic forces of a tensorial order higher than the second occur; hence, we may write quite generally,

$$\sigma = \sum_{i=1}^{m_0} J_i X_i + \sum_{i=1}^{m_1} \bar{J}_i \cdot \bar{X}_i + \sum_{i=1}^{m_2} \bar{\bar{J}}_i : \bar{\bar{X}}_i \qquad [A1]$$

Where σ = entropy production,

J_i, $\bar{J}_i$, $\bar{\bar{J}}_i$ are fluxes of the zeroth, first and second orders, respectively

and X_i, $\bar{X}_i$, $\bar{\bar{X}}_i$ are thermodynamic forces of the zeroth, first and second orders, respectively.

Any second order tensor $\bar{\bar{A}}$ may be rewritten as:

$$\begin{bmatrix} A_{11} & A_{12} & A_{13} \\ A_{21} & A_{22} & A_{23} \\ A_{31} & A_{32} & A_{33} \end{bmatrix} = \frac{1}{3} \begin{bmatrix} 1 & 0 & 0 \\ 0 & 1 & 0 \\ 0 & 0 & 1 \end{bmatrix} +$$

$$+\frac{1}{2}\begin{bmatrix} 2(A_{11}-\frac{1}{3}\,\mathrm{Tr}\,\bar{\bar{A}}) & A_{12}+A_{21} & A_{13}+A_{31} \\ A_{21}+A_{12} & 2(A_{22}-\frac{1}{3}\,\mathrm{Tr}\,\bar{\bar{A}}) & A_{23}+A_{32} \\ A_{31}+A_{13} & A_{32}+A_{23} & 2(A_{33}-\frac{1}{3}\,\mathrm{Tr}\,\bar{\bar{A}}) \end{bmatrix}$$

$$+\frac{1}{2}\begin{bmatrix} 0 & A_{12}-A_{21} & A_{13}-A_{31} \\ A_{21}-A_{12} & 0 & A_{23}-A_{32} \\ A_{31}-A_{13} & A_{32}-A_{23} & 0 \end{bmatrix} \qquad [A2]$$

i.e. $\bar{\bar{A}} = \frac{1}{3}(\mathrm{Tr}\,\bar{\bar{A}})\bar{\bar{I}} + \overset{\circ}{\bar{\bar{A}}}(s) + \bar{\bar{A}}(a)$

$$\bar{\bar{J}}_i:\bar{\bar{X}}_i = \left[\tfrac{1}{3}(\mathrm{Tr}\,\bar{\bar{J}}_i)\bar{\bar{I}} + \overset{\circ}{\bar{\bar{J}}}_i(s) + \bar{\bar{J}}_i(a)\right] : \left[\tfrac{1}{3}(\mathrm{Tr}\,\bar{\bar{X}}_i)\bar{\bar{I}} + \overset{\circ}{\bar{\bar{X}}}_i(s) + \bar{\bar{X}}_i(a)\right]$$

i.e. $$\bar{\bar{J}}_i:\bar{\bar{X}}_i = \tfrac{1}{3}(\mathrm{Tr}\,\bar{\bar{J}}_i)(\mathrm{Tr}\,\bar{\bar{X}}_i) + \overset{\circ}{\bar{\bar{J}}}_i(s):\overset{\circ}{\bar{\bar{X}}}_i(s) + \bar{\bar{J}}_i(a):\bar{\bar{X}}_i(a) \qquad [A3]$$

however, $\bar{\bar{J}}_i(a):\bar{\bar{X}}_i(a)$ may by inspection be identified with a scalar product of two axial vectors. Using this fact, substituting [A3] in [A1], collecting like terms and retaining only one term of each catagory for convenience, we obtain:

$$\sigma = J^s X^s + \bar{J}^p \cdot \bar{X}^p + \bar{J}^a \cdot \bar{X}^a + \bar{\bar{J}}^t : \bar{\bar{X}}^t \qquad [A4]$$

where the super-scripts have the following meanings:

s - Scalar p - Polar vector a - Axial vector

t - Symmetric traceless tensor

Phenomenologically speaking, the fluxes may be expressed as a sum of bilinear terms such as $L(\cdot)X$ where L is a phenomenological coefficient. In particular, heat flux may

be written as:

$$\bar{J}^{p}_{(q)} = \bar{L}^{ps}\bar{X}^{s} + \bar{\bar{L}}^{pp} \cdot \bar{X}^{p} + \bar{\bar{L}}^{pa} \cdot \bar{X}^{a} + \bar{\bar{\bar{L}}}^{pt} : \bar{X}^{t} \qquad [A5]$$

It may easily be shown that $\bar{L}^{ps}$, $\bar{\bar{L}}^{pp}$ and $\bar{\bar{\bar{L}}}^{pt}$ are polar tensors, while $\bar{\bar{L}}^{pa}$ is an axial tensor[1].

$\bar{\bar{L}}^{pp}$ is easily recognized by comparison to the well known Fourier's Law of heat conduction as a coefficient proportional to the thermal conductivity matrix, $\bar{\bar{k}}$. In fact, $\bar{\bar{L}}^{pp} = \bar{\bar{k}}T^{2}$, where T is the absolute temperature.

We shall now proceed to obtain the most general L^{pp} by using symmetry and isotropy of the thermal conductivity tensor.

To start with, let

$$\bar{\bar{L}}^{pp} = \begin{bmatrix} L_{11} & L_{12} & L_{13} \\ L_{21} & L_{22} & L_{23} \\ L_{31} & L_{32} & L_{33} \end{bmatrix} \doteq \bar{\bar{L}}. \qquad [A6]$$

Let us now subject $\bar{\bar{L}}$ to an orthogonal transformation defined by $\bar{\bar{C}}$ to transform it into $\bar{\bar{L}}^{1}$. $\bar{\bar{C}}$ is given by:

$$\bar{\bar{C}} = \begin{bmatrix} c_1^{\,1} & c_1^{\,2} & c_1^{\,3} \\ c_2^{\,1} & c_2^{\,2} & c_2^{\,3} \\ c_3^{\,1} & c_3^{\,2} & c_3^{\,3} \end{bmatrix}, \quad C = \det \bar{\bar{C}} \qquad [A7]$$

The transformation may be written as:

$$L^{1}_{ij} = C^{N} c_i^{a} c_j^{b} L_{ab} \qquad [A8]$$

where, N = weight of the tensor

$= 0$, because $\overline{\overline{L}}$ is polar.

The following example illustrates the notation used in [A8]:

$$L_{12}{}^{1} = C_1{}^{1}\, C_2{}^{1}\, L_{11} + C_1{}^{1}\, C_2{}^{2}\, L_{12} + C_1{}^{1}\, C_2{}^{3}\, L_{13}$$
$$+ C_1{}^{2}\, C_2{}^{1}\, L_{21} + C_1{}^{2}\, C_2{}^{2}\, L_{22} + C_1{}^{2}\, C_2{}^{3}\, L_{23}$$
$$+ C_1{}^{3}\, C_2{}^{1}\, L_{31} + C_1{}^{3}\, C_2{}^{2}\, L_{32} + C_1{}^{3}\, C_2{}^{3}\, L_{33}. \qquad [A9]$$

For an arbitrary notation in the 1-2 plane through an angle θ

$$\overline{\overline{C}} = \begin{bmatrix} \cos\theta & -\sin\theta & 0 \\ \sin\theta & \cos\theta & 0 \\ 0 & 0 & 1 \end{bmatrix}, \quad C = 1 \qquad [A10]$$

For $\theta = \pi,\ \pi/2$; we obtain:

$$\overline{\overline{L}}^{1} = \begin{bmatrix} L_{11} & L_{12} & -L_{13} \\ L_{21} & L_{22} & -L_{23} \\ -L_{31} & -L_{32} & L_{33} \end{bmatrix} \text{ and } \overline{\overline{L}}^{11} = \begin{bmatrix} L_{22} & -L_{21} & -L_{23} \\ -L_{21} & L_{11} & L_{13} \\ -L_{32} & L_{31} & L_{33} \end{bmatrix}$$

however a tensor remains invariant upon orthogonal transformation

$$\overline{\overline{L}} = \overline{\overline{L}}^{1} \qquad [A11]$$

and $$\overline{\overline{L}} = \overline{\overline{L}}^{11} \qquad [A12]$$

Hence from [A11], $L_{13} = -L_{13}$, $L_{23} = -L_{23}$, $L_{31} = -L_{31}$ and

$L_{32} = -L_{32}$

$L_{13} = 0$, $L_{23} = 0$, $L_{31} = 0$ and $L_{32} = 0$.

and A12 yields, $L_{11} = L_{22}$, $L_{12} = -L_{21}$

Therefore, the most general form of $\overline{\overline{L}}^{pp}$ is

$$\overline{\overline{L}}^{pp} = \overline{\overline{L}} = \begin{bmatrix} L_{11} & L_{12} & 0 \\ -L_{12} & L_{11} & 0 \\ 0 & 0 & L_{33} \end{bmatrix} \qquad [A13]$$

In the absence of a magnetic field, the Onsager relations may be written as: $\overline{\overline{L}} = \overline{\overline{\text{Ł}}}$ [A14]

where Ł is such that, $\overline{\overline{L}}_{ij} = \overline{\overline{\text{Ł}}}_{ji}$ [A15]

hence by [A14], $\begin{bmatrix} L_{11} & L_{12} & 0 \\ -L_{12} & L_{11} & 0 \\ 0 & 0 & L_{33} \end{bmatrix} = \begin{bmatrix} L_{11} & -L_{12} & 0 \\ L_{12} & L_{11} & 0 \\ 0 & 0 & L_{33} \end{bmatrix}$

which can be true only if $L_{12} = 0$ [A16]

Furthermore, since the thermal conductivity of a gas is isotropic in the absence of external fields, $L_{11} = L_{33}$ A17

Hence in the field free case,

$$\overline{\overline{L}}^{pp} = \begin{bmatrix} L_{11} & 0 & 0 \\ 0 & L_{11} & 0 \\ 0 & 0 & L_{11} \end{bmatrix} \qquad [A18]$$

In the presence of a magnetic field H, such that,

$$\overline{H} = [0, 0, H] , \qquad [A19]$$

the Onsager relations are modified to

$$\overline{\overline{L}}(H) = \overline{\overline{\text{Ł}}}(-H) \qquad [A20]$$

$$\text{i.e.,}\quad \overline{\overline{L}}^{(s)}(H) = \overline{\overline{L}}^{(s)}(-H)$$
$$\overline{\overline{L}}^{(a)}(H) = -\overline{\overline{L}}^{(a)}(-H) \qquad \text{[A21]}$$

$$\text{where}\quad \overline{\overline{L}}^{(s)} = \frac{1}{2}(\overline{\overline{L}} + \overline{\overline{L}}')$$
$$\overline{\overline{L}}^{(a)} = \frac{1}{2}(\overline{\overline{L}} - \overline{\overline{L}}') \qquad \text{[A22]}$$

Equations [A22] may be rewritten as:

$$\overline{\overline{L}}^{(s)} = \frac{1}{2}\begin{bmatrix} L_{11}+L_{11} & L_{12}-L_{12} & 0 \\ -L_{12}+L_{12} & L_{11}+L_{11} & 0 \\ 0 & 0 & L_{33}+L_{33} \end{bmatrix}$$

$$= \begin{bmatrix} L_{11} & 0 & 0 \\ 0 & L_{11} & 0 \\ 0 & 0 & L_{33} \end{bmatrix} \qquad \text{[A23]}$$

$$\text{and } \overline{\overline{L}}^{(a)} = \frac{1}{2}\begin{bmatrix} L_{11}-L_{11} & L_{12}+L_{12} & 0 \\ -L_{12}-L_{12} & L_{11}-L_{11} & 0 \\ 0 & 0 & L_{33}-L_{33} \end{bmatrix}$$

$$= \begin{bmatrix} 0 & L_{12} & 0 \\ -L_{12} & 0 & 0 \\ 0 & 0 & 0 \end{bmatrix} \qquad \text{[A23]}$$

applying [A21] to [A23] gives,

$$L_{11}(H) = L_{11}(-H),\quad L_{33}(H) = L_{33}(-H)$$
$$\text{and}\quad L_{12}(H) = -L_{12}(-H) \qquad \text{[A24]}$$

or, introducing the components of the thermal conductivity matrix,

$$k^{\perp}(H) = k^{\perp}(-H), \qquad k^{\parallel}(H) = k^{\parallel}(-H)$$
$$\text{and} \quad k^{T}(H) = -k^{T}(-H). \qquad [A25]$$

In other words, $k^{\perp}$ and $k^{\parallel}$ are even in the field while k^{T} is odd in the field. These conclusions have been proved experimentally [2], [3].

II. APPLICATION TO VARIOUS CONCENTRIC CYLINDER TYPE OF CELLS IN DIFFERENT ORIENTATIONS WITH RESPECT TO THE FIELD.

When there is no magnetic field present, the rate of heat conduction, Q, from the inner cylinder (the hotter one) to the outer cylinder (the colder one) of the cell described in Chapter II is given by:

$$Q = \frac{2\pi L(T_i - T_o)k_G}{\ln(\frac{r_o}{r_i})} \qquad [A26]$$

where k_G is the zero field thermal conductivity of gas in the continuum domain, L is the length of the cell, and r_i and r_o are the radii and T_i and T_o are the temperatures of the inner and outer cylinders, respectively.

Recall,

$$k_G = \frac{L_{11}}{T^2} \qquad [A27]$$

Equation A26 may be rewritten in the form:

$$\bar{q}_i = A\, k_G\, (\frac{\bar{dT}}{dX_i}) \qquad [A28]$$

where A is a constant.

When the field is switched on, due to the presence of transverse coefficients, a more complicated expression must be used, namely

$$\bar{q}_i = k \cdot (\bar{\nabla} T) \qquad [A29]$$

Let us now consider two cases:

a) The field $\bar{H}$ is defined by $H = [0, 0, H]$ as in the superconducting magnet. Then [A29] may be rewritten as:

$$\begin{bmatrix} q_1 \\ q_2 \\ q_3 \end{bmatrix} = A \begin{bmatrix} k_{11} & k_{12} & 0 \\ -k_{12} & k_{11} & 0 \\ 0 & 0 & k_{33} \end{bmatrix} \begin{bmatrix} \partial T/\partial x_1 \\ \partial T/\partial x_2 \\ \partial T/\partial x_3 \end{bmatrix} \qquad [A30]$$

i.e., $$q_1 = A\left(k_{11} \frac{\partial T}{\partial x_1} + k_{12}^T \frac{\partial T}{\partial x_2}\right)$$

$$q_2 = A\left(k_{11} \frac{\partial T}{\partial x_2} + (-k_{12}^T) \frac{\partial T}{\partial x_1}\right)$$

$$q_3 = A\, k_{33} \frac{\partial T}{\partial x_3} = 0$$

From the equations we can see that in this case the transverse components, k_{12} and $-k_{12}$, will not make any net contribution towards the change in thermal conductivity. k_{33} does not contribute either, because $\partial T/\partial x_3$ is zero in this orientation. Thence, the Senftleben-Beenakker effect measurement gives us the change k_{11} (or k_G) alone. See Figure 1.

b) The field $\bar{H}$ is defined by $\bar{H} = [H, 0, 0]$ as in the electromagnet. Then [A29] takes the form

$$\begin{bmatrix} q_1 \\ q_2 \\ q_3 \end{bmatrix} = A \begin{bmatrix} k_{11} & 0 & 0 \\ 0 & k_{33} & \\ 0 & k_{32} & k_{33} \end{bmatrix} \begin{bmatrix} \partial T/\partial x_1 \\ \partial T/\partial x_2 \\ \partial T/\partial x_3 \end{bmatrix} \qquad [A31]$$

i.e., $q_1 = A\, k_{11} \left(\frac{\partial T}{\partial x_1}\right)$

$$q_2 = A\left[k_{33} \left(\frac{\partial T}{\partial x_2}\right) + (-k_{32}^T)\left(\frac{\partial T}{\partial x_3}\right)\right] = A\, k_{33} \left(\frac{\partial T}{\partial x_2}\right)$$

$$q_3 = A\left[k_{32}^T \left(\frac{\partial T}{\partial x_2}\right) + k_{33} \left(\frac{\partial T}{\partial x_3}\right)\right] = A\, k_{32}^T \left(\frac{\partial T}{\partial x_2}\right)$$

Since $\partial T/\partial x_3$ is zero, the net contribution towards the measured Senftleben-Beenakker Effect comes from k_{11} and k_{33} only. In fact, because of complete radial symmetry of our cell, the measurements would yield the change in $\frac{1}{2}(k_{11} + k_{33})$ (or using another notation, $\frac{1}{2}(k_G + k_G)$). Figure 2 shows these conclusions graphically.

APPENDIX B

THE RELATIONSHIP OF THE SENFTLEBEN-BEENAKKER EFFECT TO EXPERIMENTALLY MEASURED QUANTITIES

The electrical energy, Q, supplied to the IC heater is transformed into heat and dissipated via several different paths. Most of the heat flows from the IC to the OC by conduction through the sample gas. Let this energy transfer be denoted by Q_G. The remainder of the heat may be lumped under the symbol Q_L. It may be thought of as including the heat conducted from the IC heater to the cooler parts of the probe by the ES, the T1 and the ICH leads. Hence, we may write

$$Q = Q_G + Q_L \qquad [B1]$$

Q_G may be expressed as $S\ k_G\ \Delta T$, where S is a shape factor for simple radial heat flow, k_G is the thermal conductivity of the sample gas, and ΔT is the temperature gradient across the cell. Q_L may similarly be expressed as $K_L\ \Delta T$, provided that we do not include convective and radiative transport, because they are not linear in ΔT.* This however does not represent a serious difficulty because calculations show convection to be absent and that radiative transport is very small indeed (refer to Chapter V).

Hence, by substitution

$$Q = S\ k_G\ \Delta T + K_L\ \Delta T \qquad [B2]$$

*$K_L(T)$ may be used and radiation and convection included in the same equations with negligible error for the conditions used.

In the presence of a magnetic field, if the total heat input to the cell remains constant, we may write,

$$Q = S(k_G + \delta k_G)\ (\Delta T + \delta T) + (K_L + \delta K_L)\ (\Delta T + \delta T) \quad [B3]$$

Here δk_G, δT and δK_L represent the peturbations in k_G, ΔT, and K_L caused by the field. We shall not carry δK_L along through this development because we shall assume that it is taken care of when the experiment is repeated with an inert gas.

Hence,

$$Q = S(k_G + \delta k_G)\ (\Delta T + \delta T) + K_L(\Delta T + \delta T) \quad [B4]$$

From equations [B2], [B4] we obtain

$$\frac{\Delta T}{\Delta T + \delta T} = \frac{S(k_G + \delta k_G) + K_L}{S\ k_G + K_L}$$

Since $\delta T << \Delta T$, we get,

$$\frac{S\delta k_G}{Sk_G + K_L} = -\left[\frac{\delta T}{\Delta T}\right]$$

or $$\frac{\delta k_G}{k_G} = -\left[\frac{\delta T}{\Delta T}\right]\left(1 + \frac{K_L}{Sk_G}\right)$$

By further rearrangement,

$$\frac{\delta k_G}{k_G} = -\left[\frac{\delta T}{\Delta T}\right]\left[1 - \frac{K_L}{Sk_G + K_L}\right]^{-1} \quad [B5]$$

But, by equation [B2], $Sk_G + K_L = (Q/\Delta T)_G$.

Similarly, from experiment we can obtain

$$K_L = (Q/\Delta T)_E \quad [B6]$$

The subscript "E" denoting that the cell is evacuated.

So finally, we obtain,

$$\frac{\delta K_G}{k_G} = -\left[\frac{\delta T}{\Delta T}\right]\left[1 - \frac{(Q/\Delta T)_G}{(Q/\Delta T)_E}\right]^{-1} \qquad [B7]$$

The left side, which represents a measure of the magnitude of the Senftleben-Beenakker effect is therefore expressed in terms of experimentally measured quantities δT, ΔT, $(Q/\Delta T)_G$, and $(Q/\Delta T)_E$. An equation for obtaining the gas thermal conductivity also follows easily.

From equations (B2) and B6), we have

$$Sk_G = \left\{\left[\frac{Q}{T}\right]_G - \left[\frac{Q}{T}\right]_E\right\} \qquad [B8]$$

Equation [B8] relates the thermal conductivity of the gas to experimentally measurable $(Q/\Delta T)_G$ and $(Q/\Delta T)_E$.

APPENDIX C

CALIBRATION OF THE THERMISTORS

In general, as mentioned in Chapter IV, thermistors are greatly influenced by thermal cycling, aging and various environmental conditions. Hence it is imperative to recalibrate them for each experimental run. However, the investigator was fortunate in haveing a couple of aged thermistors for which no appreciable change in calibration was noticed upon temperature cycling. It was, therefore, possible to use calibration data obtained during some calibration runs made on the superconducting magnet during May, 1968. An additional benefit of this was that the design of the probe was greatly simplified.

During the above mentioned runs the thermistors were placed in intimate thermal contact with a platinum resistance thermometer. The temperature of the probe was controlled by the use of a 3-mode automatic temperature controller. (Leeds and Northrup Model Number 60). The resistances of the thermistor being calibrated and the platinum resistance thermometer were measured simultaneously. The thermometer used was supplied by Electric Thermometer, Inc. (type G-20); along with four calibration points ranging from $83^{o}K$ to $373^{o}K$. These points were fitted to the usual Callender-Van Dusen type equation with the help of a computer program. For further

details, the reader is referred to the M.S. Thesis by L. E. Stein[36].

The calibration for T1 obtained by this method in the temperature range 77°K to 82°K is presented in Figure 10. The calibration could have been linearized by plotting log R_{T1} versus $1/T$[36].

It must be noted that the calibration curve obtained may be off by as much as ± 0.2°K in predicting the absolute temperature due to systematic errors. But, an error this size is acceptable because we are interested in measuring temperature differences accurately and not absolute temperatures. Secondly, a good calibration is necessary only for thermistor T1, because only T1 changes in temperature in response to the Senftleben-Beenakkar effect. On the other hand, T2, being on the OC, remains at a constant temperature; hence, does not require a calibration.

NOMENCLATURE

A = a constant

a_i = translational accomodation coefficient of the inner cylinder.

a_G = effective translational accomodation coefficient of the cell

B = a constant

$\overline{\overline{C}}$ = orthogonal transformation matrix

$\overline{C}$ = reduced thermal viscosity

C = determinant of $\overline{\overline{C}}$

E_i = translational energy possessed by a molecule incident to a wall

E_r = translational energy possessed by a molecule reflected by a wall

E_w = translational energy possessed by a molecule that has completely adjusted to the temperature of the wall it is reflected from

g = a factor related to the temperature jump

g_L = Landé g-factor

$\overline{H}$ = the magnetic field vector

H = magnetic field strength

$\overline{\overline{I}}$ = the unit matrix

$\overline{J}$ = reduced angular momentum

J_i = generalized flux

$J^p_{(q)}$ = heat flux

K_L = effective thermal conductivity of the heat leak paths

Kn = Knudsen number

k, k_G = thermal conductivity of the gas

k_o = thermal conductivity of the gas at zero field

k_H = thermal conductivity of the gas at field H

$\overline{\overline{L}}$ = phenomenological coefficient matrix

L = length of the cell

$\overline{\overline{L}}^1, \overline{\overline{L}}^{11}$ = transformed forms of L

l = mean free path length

m = mass of the gas molecules

N = tensorial weight

p = pressure of the gas

Q = heat input to the inner cylinder by the heater

Q_G = heat transferred by conduction through the gas

Q_L = total heat leak

Q_{RAD} = heat transferred by radiation

Q_T = total heat input to the inner cylinder

Q_{TH} = heat input by the thermistor mounted on the inner cylinder

R = a constant

δR_m = magnitude of the magnetoresistance effect.

$\delta R_{m(T1 - T2)}$ = difference between the magnetoresistance effects of T1 and T2

R_{T1} = resistance of the thermistor mounted on the inner cylinder, IC

R_{T2} = resistance of the thermistor mounted on the lower thermal anchor, TA_1

S = shape factor for the cell

T = absolute temperature of the gas

T_i = temperature of the inner cylinder, IC

= temperature corresponding to E_i (Chapter V only)

T_o = temperature of the outer cylinder, OC

T_r = temperature corresponding to E_r

T_w = temperature corresponding to E_w

ΔT = (Ti - To)

ΔT_E = temperature differential across the cell when evacuated

ΔT_G = temperature differential across the cell when filled with gas

$\bar{v}$ = velocity vector

X_i = generalized thermodynamic force

α = the angle between $\bar{v}$ and $\bar{\mu}$

β = non-sphericity parameter

μ = angular momentum vector

σ = entropy production (Appendix A only)
= hard sphere diameter

τ = time between collisions

τ_c = characteristic time for a collision process

Ω^{ls}, $\Omega^{(l,s)}$ = the Omega integrals

$\Omega^{(l,s)*}$ = dimensionless Omega integrals

$\Omega_{HS}^{(l,s)}$ = hard sphere Omega integral

ω_L = Larmor precession frequency

C = stainless steel cylinder

D = dewar

ES = end seals

FT = feed through

FT_1 = fill tube

GT = glass tube

IC = inner cylinder

ICH = inner cylinder heater

LF = lower flange

OC = outer cylinder

OT = outer stainless steel tube

P = plug

PP = porous paper

RS = radiation shield

S = sleeve

T = stainless steel tube

T1 = thermistor mounted on IC

T2 = thermistor mounted on TA

TA_1 = lower thermal anchor

TA_2 = upper thermal anchor

TS = teflon spacer

UF = upper flange

BIBLIOGRAPHY

1. De Groot, S. R. and P. Mazur, "Non-Equilibrium Thermodynamics" (North-Holland Publishing Co., Amsterdam, 1962)

2. Hermans, L. J. F., P. H. Fortuin, H. F. P. Knapp, and J. J. M. Beenakker. Phys. Letters 25A, 2 (1967).

3. Hermans, L. J. F., A. Schutte, H. F. P. Knapp and J. J. M. Beenakker. Physica 44, 123 (1968).

4. Beenakker, J. J. M., G. Scoles, H. F. P. Knapp and R. M. Jonkman. Phys. Letters 2, 5 (1962).

5. Senftleben, H. Phys. Z. 31, 961 (1930).

6. Senftlebeh, H. and H. Gladisch. Ann. Physik 30, 713 (1937); ibid. 33, 471 (1938).
H. Enguelhardt and H. Sach. Phys. Z. 33, 724 (1932).
M. Trantz and E. Froschel. Phys. Z. 33, 947 (1932).

7. Senftleben H. and Piezner. Ann. Physik. 16, 907 (1933); ibid. 27, 108, 117 (1936); ibid. 30, 541 (1937).
E. Reiger. Ann. Physik 31, 453 (1938).
H. Torwegge. Ann. Physik 33, 947 (1932).

8. Scott, G. G., H. W. Stenner and R. M. Williamson, Phy. Rev. 158, 117 (1967).

9. Gorter, C. J. Naturwiss. 26, 140 (1938).

10. Zernike, F. and van Lier. Physica 6, 961 (1939).

11. Korving, J., H. Hulsman, H. F. P. Knapp and J. J. M. Beenakker. Phy. Letters 17, 33 (1965); ibid. 21, 5 (1966).

12. Honeywell, W. I., J. Korving and J. J. M. Beenakker. Physica 36, 177 (1967).

13. Kagan, Y. and L. Maksimov. Soviet Phys. JETP 14, 604 (1962).
ibid. 24, 1272 (1967).

14. Waldman, L. Z. Naturforsch 18a, 1033 (1963).

15. Kagan, Y. and A. M. Afans'ev. Soviet Phys. JETP 14, 1096 (1962).

16. Dahler, J. S. and N. F. Sather. J. Chem. Phys. 38, 2363 (1962).

17. Sandler, S. I. and J. S. Dahler. J. Chem. Phys. 43, 1750 (1965)
ibid. 44, 1229 (1966).

18. Condiff, D. W., W. K. Lu and J. S. Dahler. J. Chem. Phys. 42, 3445 (1965).

19. McCoy, B. J., S. I. Sandler and J. S. Dahler. J. Chem. Phys. 45, 3485 (1966).

20. Dahler, J. S. J. Chem. Phys. 30, 1447 (1959).

21. Snider, R. F. J. Chem. Phys. 32, 1051 (1960).

22. McCourt, F. R. "Transport Properties of Gases with Rotational States", Ph.D. dissertation, University of British Columbia, Vancouver, Canada, 1966.

23. McCourt, F. R. and R. F. Snider. J. Chem. Phys. 46, 2387 (1967).
ibid. 43, 2276 (1965).

24. Chapman, S. and T. G. Cowling. "The Mathematical Theory of Non-Uniform Gases". (Cambridge University Press, London, 1952).

25. Knapp, H. F. P. and J. J. M. Beenakker., Physica 33, 643 (1967).

26. Hess, S. and Waldman, L., Z. Naturforsch 21a, 1529 (1966).

27. Gorelik, L. L., V. G. Nikolaevskiz, and V. V. Sinitsyn, Soviet Phys. JETP 4, 307 (1966).

28. Kagan, Y. M. and L. A. Maksimov, Soviet Phys. JETP 24, 1272 (1967).

29. Korving. J., H. F. P. Knapp, R. G. Gordon, and J. J. M. Beenakker. Phy. Letters, 24A, 755 (1967).

30. Hirschfelder, J. O., C. F. Curtiss and R. B. Bird. "Molecular Theory of Gases and Liquids." (John Wiley, New York, 1954).

31. Beenakker, J. J. M., "The Transport Properties of Polyatomic Gases", lecture notes.

32. Korving J. "The Influence of Magnetic Field on the Properties of Gases of Polyatomic Molecules", Ph.D. Dissertation, Leiden University, Leiden, Holland, 1966.

33. Knudsen, M. "Kinetic Theory of Gases" (Methuen and Co., Ltd., London, 1934).

34. Kennard, E. H. "Kinetic Theory of Gases" (McGraw Hill Book Co., Inc., New York, 1938).

35. Elliot, D. G. "A Cell for Measuring the Influence of Magnetic Fields on the Thermal Conductivity of Gases." M.S. Thesis, University of Houston, Houston, USA. 1969.

36. Stein, L. E. "A Low Temperature Investigation of the Effect of Magnetic Fields on the Resistance Characteristics of a Thermistor" M.S. Thesis, University of Houston, Houston, USA, 1969.

37. Camp, F. W., E. F. Johnson. I. & E.C. Fundamentals 4, 2 (1965).

38. Jakob, M., G. A. Hawkins. "Elements of Heat Transfer" (John Wiley, New York, 1957).

39. Devienne, F. M. Advances in Heat Transfer 2, 271 (1965).

40. Guthrie, A. "Vacuum Technology" (John Wiley, New York, 1965).

41. Hermans, L. J. F., J. M. Koks, A. F. Hengeveld and H. F. P. Knapp. To be published in Physica 46 (1970).

42. Childs, G. E. and J. M. Hanley. "The Thermal Conductivity Coefficients of Dilute Nitrogen and Oxygen." NBS Tech. Note 350 (1966).

43. Chan, S. I., M. R. Baker and N. F. Ramsey. Phys. Rev. 136, 1224 (1964).

44. Springer, G. S. and R. Ratonyi. Trans. of ASME 65, 4 (1965).